AD-A279 944

PAGE

Form Approved
OMB No. 0704-0188

Public reporting ... gathering and ... collection of info... Davis Highway, S... ...or reviewing instructions, searching existing data sources, ...of information. Send comments regarding this burden estimate or any other aspect of this ...Headquarters Services, Directorate for Information Operations and Reports, 1215 Jefferson ...and Budget, Paperwork Reduction Project (0704-0188), Washington, DC 20503.

1. AGENCY USE ONLY (Leave blank)	2. REPORT DATE	3. REPORT TYPE AND DATES COVERED
	5/3/94	Final Report: 11/15/90 - 02/14/94

4. TITLE AND SUBTITLE

Final Report: Prediction of Global Cloud Cover with a very High Resolution Global Spectral Model

5. FUNDING NUMBERS

AFOSR-91-0023

61102F 2310/A1

6. AUTHOR(S)

Dr. T.N. Krishnamurti

7. PERFORMING ORGANIZATION NAME(S) AND ADDRESS(ES)

Department of Meteorology 3034
Florida State University
Tallahassee, FL 32306-3034

8. PERFORMING ORGANIZATION REPORT NUMBER

AFOSR-TR- 94 0334

9. SPONSORING/MONITORING AGENCY NAME(S) AND ADDRESS(ES)

AFOSR/NC
Bldg. 410
Bolling AFB, DC 20332-6448
Maj James Kroll

10. SPONSORING/MONITORING AGENCY REPORT NUMBER

AFOSR-91-0023

11. SUPPLEMENTARY NOTES

12a. DISTRIBUTION/AVAILABILITY STATEMENT

Approved for public release;
distribution unlimited.

12b. DISTRIBUTION CODE

13. ABSTRACT (Maximum 200 words)

The completed research is in the area of cloud prediction with a high resolution global model. We have extended our studies on the handling of implicit clouds (i.e. clouds specified as a function of prevailing humidity). We have also examined this problem in the context of rainfall initialization (called physical initialization). We demonstrate a strong positive impact on cloud forecasts from such an initialization. We have also made a start on the problem of explicit cloud forecasts using cloud water mixing ratio and cloud fractions as basic forecast variables. Our preliminary results, described in the final report, are very encouraging. Mannoji (1994) has in fact noted a slight superiority of the explicit over the implicit scheme. That work was performed using a low resolution global model. Further work on the improvement of the explicit scheme at higher resolution is required.

14. SUBJECT TERMS

Cloud prediction, global modelling of clouds.

15. NUMBER OF PAGES

10 pp. + appendix

16. PRICE CODE

17. SECURITY CLASSIFICATION OF REPORT	18. SECURITY CLASSIFICATION OF THIS PAGE	19. SECURITY CLASSIFICATION OF ABSTRACT	20. LIMITATION OF ABSTRACT
U	U	U	U

AFOSR-TR- 94 0334

The Florida State University
Tallahassee, Florida 32306-3034
Department of Meteorology
Phone # (904) 644-6205
Fax # (904) 644-9642

Approved for public release;
distribution unlimited.

May 3, 1994

Major James Kroll
AFOSR/NL
110 Duncan Avenue
STEB 115
Bolling AFB, DC 20332

DTIC
ELECTE
JUN 06 1994
S D
G

Re: AFOSR–91–0023

Dear Major Kroll,

Please find enclosed our final technical report covering the entire three year project entitled "Prediction of Global Cloud Cover with a very high Resolution Global Spectral Model".

If any further information is required, please feel free to contact me at 904–644–2210, fax 904–644–9642 or e–mail TNK@cloud1.met.fsu.edu.

We sincerely appreciate the continued Air Force support for our research efforts.

Sincerely,

T N Krishnamurti

T.N. Krishnamurti

TNK/sam

Encl.

cc: Sally Gavins (1338–625–27)

DTIC QUALITY INSPECTED 3

94-16602

94 6 3 047

MAY 1994

Accesion For
NTIS CRA&I
DTIC TAB
Unannounced
Justification
By
Distribution /
Availability Codes
Dist | Avail and / or Special
A-1

Prediction of Global Cloud Cover with a Very High Resolution Global Spectral Model

Work Completed

A. Implicit Clouds:

We have made considerable progress in the area of implicit treatment of clouds. This improvement resulted partly from involving physical initialization prior to the global model forecast experiments. A review of this work appears in Appendix 1 of this proposal.

a) Physical Initialization:

When we examine the frequencies of a complete atmospheric nonhydrostatic model we find that acoustic waves, gravity and slow moving atmospheric Rossby waves are the principal modes. Errors in the initial data analysis, especially of the mass and motion field result in the growth of the higher frequency motions. We call these computational modes. The use of hydrostatic approximation in the vertical equation of motion is adequate to suppress the acoustic waves. The suppression of high frequency computational gravity modes is usually accomplished using a normal mode initialization.

Given an initial data set which is subjected to an analysis scheme (such as optimal interpolation or variational statistical methods), an assimilation within the model's infrastructure and to the normal mode initialization one would expect to have described a reasonable initial state for the model's forecast. Such is not the case if there are major data gaps as is the case especially over the tropical latitudes and the southern hemisphere. There exist some alternate data sets such as measures of rain rates from remote sensing from satellites. Rainfall rate is not a basic dependent variable of a forecast model. It is an internal product. To incorporate rainrates into the data analysis one needs to assimilate a precipitation process consistent with the rainrates as input. That can be done using inverse algorithms that

generate proxy variables for the assimilation. This method is called physical initialization, Krishnamurti et al. (1991a).

The humidity variable is poorly described by the available observations, especially over the tropics. Physical initialization within a data assimilation restructures the vertical distribution of humidity consistent with the observed rainfall rates. This enables the model to return a rain rate nearly the same as the observed during the physical initialization within the data assimilation. During the assimilation the heating from the condensation process, the divergence distribution and the surface pressure fields adjust to the rain rates. This procedure has been found to exhibit a considerable skill in the rainfall forecasts over very short range time scales. The noteworthy improvements are in the nowcasting (day 0) and the one day forecast of rainfall over the entire tropics. Figure (1a) illustrates a 24 hour tropical rainfall distribution as measured by satellite (microwave radiometers and outgoing longwave radiation) and raingauge network, and figure (1b) illustrates the model initialization of the 24 hour rain. As is evident here a high resolution global model (Triangular truncation 170 waves) is able to initialize such rainfall very closely. These rainfall observations supplement the other conventional weather observations via the inverse algorithms. The day 0 and the one day forecast skill of rainfall is illustrated in figure (2a,b). Here we show correlation of observed and initialized (or predicted) rainfall for data over transform grid squares. Also shown in these illustrations are some correlations for operational weather centers and for our control experiments where such a physical initialization was not executed. Overall it is apparent that the rain rate initialization provides a very useful data source for the tropical latitudes. In the appendix we show a strong positive impact on cloud forecasts from physical initialization.

b) Definition of Implicit Clouds:

Clouds are classified as high, middle, and low. High clouds are defined to exist between 400 and 100 mb, middle clouds between 700 and 400 mb, and low clouds between 900 and 700 mb. Clouds are not defined for sigma levels below low cloud bases or above

high cloud tops.

The amount of a cloud type in an individual layer is assumed to be a function of the relative humidity, which is dependent on the moisture, temperature, and pressure. The clouds are assumed to be present when the mean relative humidity ($\overline{RH}$) in a layer exceeds the threshold value (RHc). The cloud amount N for each type of cloud is defined by the relation.

$$N_{(H,\ M\ or\ L)} = \left[\frac{\overline{RH} - RHc}{1 - RHc}\right]^2, \quad \overline{RH} > RHc$$

where RHc has been set to 0.25, 0.40, and 0.50 for high, medium, and low clouds, respectively. $\overline{RH}$ is the pressure weighted mean relative humidity in a layer. The maximum possible value of N is 1. The cloud amount N is set to 0, when $\overline{RH}$ is less than RHc. Total cloud amount (N_T) is determined by using random overlap of the cloud layers in a column as given by $N_T = 1 - (1-N_L)(1-N_M)(1-N_H)$. *Cloud covers* ($CC_n$) is partitioned into eight sky condition categories as defined in Krishnamurti et al. (1990):

$CC_1 = (1 - N_L) (1 - N_M) (1 - N_H)$	clear sky
$CC_2 = N_L (1 - N_M) (1 - N_H)$	low clouds only
$CC_3 = N_L N_M (1 - N_H)$	low and middle clouds
$CC_4 = N_L N_M N_H$	low, middle, and high clouds
$CC_5 = N_M (1 - N_L) (1 - N_H)$	middle clouds only
$CC_6 = N_M N_H (1 - N_L)$	middle and high clouds
$CC_7 = N_H (1 - N_L) (1 - N_M)$	high clouds only
$CC_8 = N_L N_H (1 - N_M)$	low and high clouds

This sky condition is used in the computation of the solar radiation absorbed or

scattered by clouds.

c) Treatment of Cirrus Clouds:

High level clouds (e.g. cirrus) play an important role in the atmospheric radiation budget. They allow both the short and longwave radiation to be transmitted through them partially, and therefore are treated as non-black in the radiative transfer model. Their characteristics are based on the optical depth, the single scattering albedo and the symmetry scattering factor in the radiation scheme. The optical depth of cirrus is simply assumed to be a function of temperature. The contents of cirrus categorize ice and supercooled water droplets with temperature range between 190.65 K and 263.15 K, supercooled water droplets between 263.15 K and 273.15 K. The single scattering albedo of cirrus is then determined based on the ratio of the optical depth of cirrus to the total optical depth of the atmosphere. The symmetry scattering factor is fixed as constant for clouds.

No cloud microphysics based on phase change of water is considered in the implicit cloud scheme.

d) Treatment of Tropical Clouds:

In general, cumulus clouds have horizontal scales of the order of a few kilometers, and are not explicitly resolved by large scale numerical weather prediction models. Cumulus parameterization was needed to address this issue. Our cumulus parameterization for deep cloud in a tropical region is based on Kuo (1974). The heating and moistening of the atmosphere and the rainfall rates of this procedure are simple functions of the large scale convergence. A further refinement of this scheme was provided by Krishnamurti and Bedi (1988a). Here statistically based improvements on the Kuo scheme were made to provide global applicability and minimization of initial errors of the heating, moistening and rainfall rates.

For convective clouds, a cloud fraction, CC, is based on the rainfall rates of a Kuo's

scheme. The past three hours of rainfall total are used to determine the cloud coverage fraction CC. Table 6 describes these relationships.

Table 5: Relationship Between the Precipitation Rates and Convective Cloud Cover in NMC Model

P (mm/day)	.14	.31	.70	1.6	3.4	7.7	17.	38.	85.
CC (fraction)	0	.1	.2	.3	.4	.5	.6	.7	.8

For rainfall rates less than 1.6 mm/day, 25% of the cloud coverage fraction for convective clouds are identified as high clouds and 75% as the low cumulus bed. However, if the rainfall exceeds 1.6 mm/day, then the cloud fraction for cirrus is given by a relation,

$$C_{cirrus} = 2 * (CC - .3)$$

This is supposed to account for the cumulonimbus anvils.

e) Treatment of Radiative Transfer:

In most models the physics algorithms include rather sophisticated parameterizations for the radiative transfer processes. The total problem includes the parameterization of short and long wave irradiances, the effects of clouds, role of atmospheric constituents such as water vapor, carbon dioxide and ozone. The definition of clouds and cloud radiative interactions are important areas in modelling. The surface energy balance is also strongly radiatively controlled since it effects issues such as the diurnal changes and land surface processes.

Most current radiative transfer models include what are called band models. The atmospheric absorption bands for the solar and the long wave irradiances are sorted out over selected representative absorption bands. This is a time saving technique and it is possible to

replicate results (for clear sky conditions) as one would obtain from line by line integrations across the entire atmospheric spectrum.

For clear skies we use the so-called k-distribution approximation following Stephens (1984) for the absorption of solar radiation. For cloudy skies we invoke a detailed multiple scattering computation based on the work of Davies (1982). Here, apart from absorption, we consider the reflection and transmission characteristics of various layers of the atmosphere. Following Joseph and Wiscombe (1976), we use the so-called Delta-Eddington approximation which is also called a two stream approximation. The ozone absorption, especially in the stratosphere, is important where the Rayleigh scattering is significant. This is mostly below the ozone layer of the stratosphere. Consideration is given to the weak visible bands (Chapius bands) and the ultraviolet bands (Hartley and Higgins bands) following the formulation of Lacis and Hansen (1974). Surface absorption is divided into two bands, one where the water vapor absorption is large and the other includes the rest of the spectrum. The parameterization of long wave irradiances follows Harshvardhan and Corsetti (1984). This includes band scaling approximations (the band-centers and band-wings) for carbon dioxide and water vapor following Chou and Peng (1983) and Chou (1984). The transmission functions for ozone are based on the formulation of Rodgers (1968). The molecular line absorption and e-type absorption (continuum absorption) of diffuse-transmittance function due to both water vapor and CO_2 are included in this analysis.

The specification of clouds in many models is based on certain threshold humidity criteria. Three types of clouds are considered: low, middle and high. If the model based predicted humidity exceeds certain thresholds then the radiatively active clouds are assumed to exist in that vertical layer of the atmosphere. Low and middle clouds are regarded as black body radiators; the high level clouds (e.g. cirrus), however, are treated as partial black body radiators.

An example of cloud-radiative interaction is presented next. Tropical oceans exhibit a very large coverage of shallow stratocumulus clouds. The atmosphere over the tropical ocean

exhibits a moist instability over the lower troposphere. The cloud base over this region lies roughly 1 km above the ocean and the cloud top is usually located near the top of this unstable region which is roughly 3 km above the ocean. The maintenance of this unstable layer is a central issue in tropical meteorology. Radiative processes and surface evaporation contribute to the steady restoration of this instability whereas convective clouds contribute towards its erosion. Tropical weather disturbances feed on this instability. If the restoring mechanisms are not properly modeled, the air entering tropical storms does not provide sufficient instability for cloud growth and storm forecasts tend to degrade. The long wave radiative cloud top cooling is one of the major mechanisms that restores conditional instability. Fig. (3a, b) illustrates results of 4 day forecasts of a storm where two different radiative parameterization methods were used in the global model. The bottom panel shows the low cloud distributions for the above band model. The upper panel illustrates the results from a classical radiation algorithm called the emissivity-absorptivity method, Chang (1980). The latter did not provide a sufficient cooling rate over the lower troposphere; the temperatures were high, the relative humidity as a consequence was too low, and low clouds did not form since the threshold value of relative humidity were not exceeded. Lacking sufficient low clouds the restoration of conditional instability was underestimated. Fig. (4) illustrates the time histories of the predicted cooling rates and humidity for these two respective radiative transfer models. In these experiments a vigorous storm did form and move over China when the band model was used, and that storm weakened and disappeared in the forecast where the emissivity-absorptivity model for cloud radiative interaction was used, Krishnamurti et al. (1991b).

f) Results from the implicit cloud scheme:

These are presented in Appendix 1.

B. Explicit Clouds:

We have made some progress in the areas of the explicit treatment of clouds. This has

required a major extension of the global model from the inclusion of two dependent variables i.e., the cloud water mixing ratio and the cloud fractions. This work is still ongoing and will form the major area of research for the new proposal. Cloud microphysical processes are crudely represented. In this scheme the time evolution of the cloud variables are determined by the sources and sinks due to the several cloud processes. This scheme considers the formation of clouds in connection with large-scale ascent, cumulus convection, and radiative cooling. Clouds dissipate through adiabatic and diabatic heating, turbulent mixing of cloud air with unsaturated environmental air, and depletion of cloud water by precipitation. Both liquid and ice phases are included in the cloud model. The liquid phase processes consist of evaporation, condensation, autoconversion and precipitation. The ice phase processes include only gravitational settling of cloud ice. Cloud water and cloud ice are presently distinguished based on the prescribed temperature but are treated as a bulk for cloud water path in the radiation scheme. Cloud processes are represented using a bulk water parameterization technique, where the liquid phase is subdivided into cloud water and precipitation water. Cloud water is assumed to form when the relative humidity exceeds a specified threshold value, and precipitation processes are described by simple empirical parameterizations for warm and cold clouds.

The advantage of this approach is that it is physically realistic and is consistent with the rest of the model, while directly accounting for the various feedbacks involving clouds. However, the accuracy of cloud parameterization within this approach depends critically on the realistic treatment of advective transport of cloud variables, subgrid-scale processes, cloud microphysics, and cloud optical properties. Note that there still exist large uncertainties in the representation of these processes. Details of these are presented in Appendix 1.

Publications Completed

Lee, H.-S., 1994: Impact of physical initialization on cloud forecasts. Master thesis, Department of Meteorology, The Florida State University, Tallahassee, Florida 32306, 97 pp.

Mannoji, N., 1994: An explicit cloud predicting scheme in the Florida State University Global Spectral Model. To appear in *J. Meteor. Soc. Japan.*

Wai, M.M.-K. and T.N. Krishnamurti, 1992: An improvement in cumulus parameterization by invoking outgoing longwave radiation. *Meteorol. Atmos. Phys.*, 50, 175-187.

References

Chang, C.B., 1980: On the influence of solar radiation and diurnal variation of surface Temperatures on African Disturbances. PhD Dissertation. Dept. of Meteorology, Florida State University, Tallahassee, FL 32306, 157 pp.

Chou, M.D., 1984: Broadband water vapor transmission functions for atmospheric IR flux computations. *J. Atmos. Sci.*, 41, 1775-1778.

Chou, M.D. and Peng, L., 1983: A parameterization of the absorption in the 15 μm CO_2 spectral region with application to climate sensitivity studies. *J. Atmos. Sci.*, 40, 2183-2192.

Davies, R., 1982: "Documentation of the Solar Radiation Parameterization in the GLAS Climate Model". NASA Tech. Memo. 83961. Goddard Space Flight Cent., Greenbelt, Maryland.

Harshvardhan, and Corsetti, T.G., 1984: "Longwave Parameterization for the UCLA/GLAS GCM", NASA Tech. Memo. 86072. Goddard Space Flight Cent., Greenbelt, Maryland.

Joseph, J.H., Wiscombe, W.J. and Weinman, J.A., 1976: The delta-Eddington approximation of radiative flux transfer, *J. Atmos. Sci.*, 33, 2452-2459.

Krishnamurti, T.N., J. Xue, H.S. Bedi, K. Ingles and D. Oosterhof, 1991a: Physical initialization for numerical weather prediction over the tropics. *Tellus*, 43AB, 53-81.

Krishnamurti, T.N., K.S. Yap and D.K. Oosterhof, 1991b: Sensitivity of Tropical Storm Forecast to Radiative Destabilization. *Mon. Wea. Rev.*, 119, 2176-2205.

Krishnamurti, T.N., A. Kumar, K.S. Yap, A.P. Dastoor, N. Davidson and J. Sheng, 1990: Performance of a High-Resolution Mesoscale Tropical Prediction Model. *Adv. Geoph.*, 32, 133-286.

Krishnamurti, T.N., and H.S. Bedi, 1988a: Cumulus Parameterization and Rainfall Rates: Part III, *Mon. Wea. Rev.*, 116, 583-599.

Kuo, H.L., 1974: Further studies of the parameterization of the influence of cumulus convection on large scale flow. *J. Atmos. Sci.*, 31, 1232-1240.

Lacis, A.A., and Hansen, J.E., 1974: A parameterization for the absorption of solar radiation in the Earth's atmosphere, *J. Atmos. Sci.*, 31, 118-133.

Rodgers, C.D., 1968: Some extensions and applications of the new random model for molecular band transmission, *Q. J. R. Meteor. Soc.*, 94, 99-102.

APPENDIX I

TABLE OF CONTENTS

LIST OF TABLES

LIST OF FIGURES

LIST OF ACRONYMS

ECMWF	European Centre for Medium Range Weather Forecasts
ERBE	Earth Radiation Budget Experiment
FSUGSM	Florida State University Global Spectral Model
GATE	GARP Atlantic Tropical Experiment
GCM	Global Circulation Model
GLAS	Goddard Laboratory of Atmospheric Science
ITCZ	Inter-Tropical Convergence Zone
LCL	Lifting Condensation Level
NMC	National Meteorological Center
NWP	Numerical Weather Prediction
OLR	Outgoing Longwave Radiation
PRMSE	Persistence Root Mean Square Error
RMSE	Root Mean Square Error
SPCZ	Southern Pacific Convergence Zone
SSM/I	Special Sensor Microwave/Imager
STP	Standard Temperature and Pressure
T106(42)	Triangular Truncation at 106(42) Waves
UCLA	University of California at Los Angeles
UTC	Universal Time Coordinate
WWW	World Weather Watch

ABSTRACT

The impact of the initial data on the cloud forecast by the Florida State University Global Spectral Model (FSUGSM) has been investigated. Additionally two different cloud schemes, one implicit, the other explicit, were tested. This work has shown that improving the information content of the initial data by physical initialization has a very strong, positive impact on cloud forecasts.

The physically-initialized data has a greater impact in the implicit cloud scheme. Model spin-up of cloud generation is considerably reduced. There is an overall better representation of high, middle, low and total clouds over the tropics and there is a discernible improvement in the prediction of clouds. A strong negative correlation between cloud shortwave forcing and longwave forcing has been observed in the implicit scheme experiments. This result matches very closely with the Earth Radiation Budget Experiment (ERBE) observations. The explicit scheme does not respond in a similar fashion. The physically-initialized data has only a minor impact on forecasts made using the explicit scheme. This suggests a need for further research into the physical initialization of explicit cloud schemes.

CHAPTER I

INTRODUCTION

Clouds are among the most important regulators of the weather and climate in the earth's atmosphere. Their importance for the atmospheric circulation has been recognized for many years. However, clouds interact with atmospheric processes (i.e., turbulence, large scale circulation and radiation) in many ways, and hence their role is still poorly understood. The lack of knowledge of cloud process has also impaired cloud parameterization in climate and forecast models.

During the last decade there has been a considerable improvement in model representation of clouds. Slingo (1987) improved model-generated cloud fields by linking clouds to atmospheric properties such as relative humidity, vertical velocity, and static stability. This scheme, the so-called implicit cloud scheme, is successful in producing some of the gross features of global cloudiness but it lacks a sound physical basis and does not represent the interaction between clouds and the hydrological cycle of the model. However, because the implicit scheme is simple, it is widely used in large-scale models. More recently, more physically realistic schemes (explicit cloud schemes) have been developed (Sundqvist, 1978: Le Treut and Li, 1989: Smith, 1990; Tiedtke, 1991, 1993; Mannoji, 1993). With these schemes cloud liquid water content and cloud cover are predicted through a prognostic equation. The advantage of this

approach is that it represents the interaction between clouds and the hydrological cycle of the model.

It has been realized (Tiedtke, 1993) that in order to improve the model representation of clouds, the information content of the initial state must also be enhanced. At present, operational data assimilation systems do not provide a robust initial state over tropical regions due to the sparsity of conventional observations. This causes low equilibration of the humidity field, which is the so-called model spin-up. It reduces forecast skill of numerical weather predictions (NWP) at the lower latitudes. Krishnamurti *et al.* (1984) proposed the physical initialization scheme which improves the initial state by assimilating observed rain rates. Physical initialization restructures the vertical distribution of humidity and constrains the evolution of divergence distribution, surface pressure fields and heating from the condensation process to be consistent with observed rain rates and model physics. In impact studies of physically initialized data sets, Krishnamurti *et al.* (1991) have shown an overall improvement in the distribution of the rainfall and a very high correlation between the observed and model forecasted rain rates. Mathur *et al.* (1992) also have shown a strong positive impact of physical initialization on tropical rain forecasts. Krishnamurti *et al.* (1994) have shown that the correlation for 1 day forecast with the physically initialized data is 0.55 which exceeds both the current operational skills of 0.2 to 0.5 and the 0.3 correlation of persistence.

It is our contention that the physically initialized data set with its enhanced information will have strong positive impact on cloud forecasts. With this intention, we designed a set of experiments to test the impact of physically initialized data set on two cloud parameterization schemes, namely, the implicit cloud scheme and explicit cloud scheme. Furthermore, we also intended to illustrate the extreme sensitivity of

cloud forecasts to the initial cloud distribution. Much of the previous related work has focused on improvements to the parameterization schemes. However, this study emphasizes the fact that the initial data is equally important in cloud forecasts. In this regard, efforts at European Center for Medium-Range Forecasts (ECMWF) are already underway to incorporate the explicit cloud scheme into the data assimilation system so that cloud variables are carried forward in time (Tiedtke, 1993).

The thesis has been divided to five chapters. The model is described in Chapter II. Physical initialization is discussed in great detail in Chapter III. The numerical experiments conducted and results are presented in Chapter IV. Finally, the conclusions are presented in Chapter V.

CHAPTER II

THE FSU GLOBAL SPECTRAL MODEL

2.1 Overview

Two versions of the Florida State University Global Spectral Model have been used in this study on cloud prediction. One involves an implicit cloud scheme, while the other utilizes an explicit cloud scheme. Full documentation of the FSUGSM is given in Krishnamurti *et al.* (1991). The FSUGSM includes the following features:

(a) Independent variables: (x, y, σ, t).

(b) Dependent variables: vorticity, divergence, surface pressure, vertical velocity, temperature and humidity.

(c) Horizontal resolution: Triangular 106 waves.

(d) Vertical resolution: 14 layers between roughly 50 and 1000 mb.

(e) Semi-implicit time differencing scheme.

(f) Envelope orography (Wallace *et al.*, 1983).

(g) Centered differences in the vertical for all variables except humidity which is handled by an upstream differencing scheme.

(h) Fourth-order horizontal diffusion (Kanamitsu *et al.*, 1983).

(i) Kuo-type cumulus parameterization (Kuo 1965, 1974; Krishnamurti *et al.*, 1983).

(j) Shallow convection (Tiedke, 1984).

(k) Dry convective adjustment.

(l) Large scale condensation (Kanamitsu, 1975).

(m) Surface fluxes via similarity theory (Businger *et al.*, 1971).

(n) Vertical distribution of fluxes utilizing diffusive formulation where the exchange coefficients are functions of the Richardson number (Louis, 1979).

(o) Long- and shortwave radiative fluxes based on the emissivity/absorptivity methods (Chang, 1979).

(p) Diurnal cycle with respect to the radiative processes.

(q) Implicit cloud: Parameterization of low, middle and high clouds based on threshold relative humidity for radiative transfer calculations (Krishnamurti *et al.*, 1991).
Explicit cloud: Parameterization of cloud water content and cloud cover (Mannoji, 1993).

(r) Surface energy balance coupled to the similarity theory (Krishnamurti et al., 1988).

The 14 level, T106 FSUGSM used in the study has a spatial resolution of approximately 0.94 degrees with 160 Gaussian latitudes and 384 Gaussian longitudes. The vertical structure is defined by the sigma coordinate. Figure 2.1 shows a schematic of the vertical structure of the 14 level model.

Implicit cloud scheme and related physical processes are described in section 2.2. A description of explicit cloud scheme is detailed in section 2.3. Section 2.4 discusses the radiative transfer processes of the model, which is a common feature in both schemes. A modification to parameterization of deep cumulus convection in the implicit cloud scheme is presented in section 2.5.

2.2 Implicit cloud scheme

2.2.1 Definition

Clouds are classified as high, middle, and low. High clouds are defined to occur between 400 and 100 mb, middle clouds between 700 and 400 mb, and low clouds

between 900 and 700 mb. Clouds are not defined for sigma levels below low cloud bases or above high cloud tops.

The amount of a cloud type in an individual layer is assumed to be a function of the relative humidity, which is dependent on the moisture, temperature, and pressure. Clouds are assumed to be present when the mean relative humidity ($\overline{RH}$) in a layer exceeds the threshold value (RHc). The cloud amount N for each type of cloud is defined by the relation.

$$N_{(H,\ M\ or\ L)} = \left[\frac{\overline{RH} - RHc}{1 - RHc}\right]^2, \quad \overline{RH} > RHc \tag{2.1}$$

where RHc has been set to 0.25, 0.40, and 0.50 for high, medium, and low clouds, respectively. $\overline{RH}$ is the pressure weighted mean relative humidity in a layer. The maximum possible value of N is 1. The cloud amount N is set to 0, when $\overline{RH}$ is less than RHc. Total cloud amount (N_T) is determined from a random overlap of the cloud layers in a column as given by $N_T = 1 - (1-N_L)(1-N_M)(1-N_H)$. Cloud coverage ($CC_n$) is partitioned into eight sky condition categories as defined in Krishnamurti *et al.* (1990):

$CC_1 = (1 - N_L) (1 - N_M) (1 - N_H)$	clear sky
$CC_2 = N_L (1 - N_M) (1 - N_H)$	low clouds only
$CC_3 = N_L N_M (1 - N_H)$	low and middle clouds
$CC_4 = N_L N_M N_H$	low, middle, and high clouds
$CC_5 = N_M (1 - N_L) (1 - N_H)$	middle clouds only
$CC_6 = N_M N_H (1 - N_L)$	middle and high clouds
$CC_7 = N_H (1 - N_L) (1 - N_M)$	high clouds only

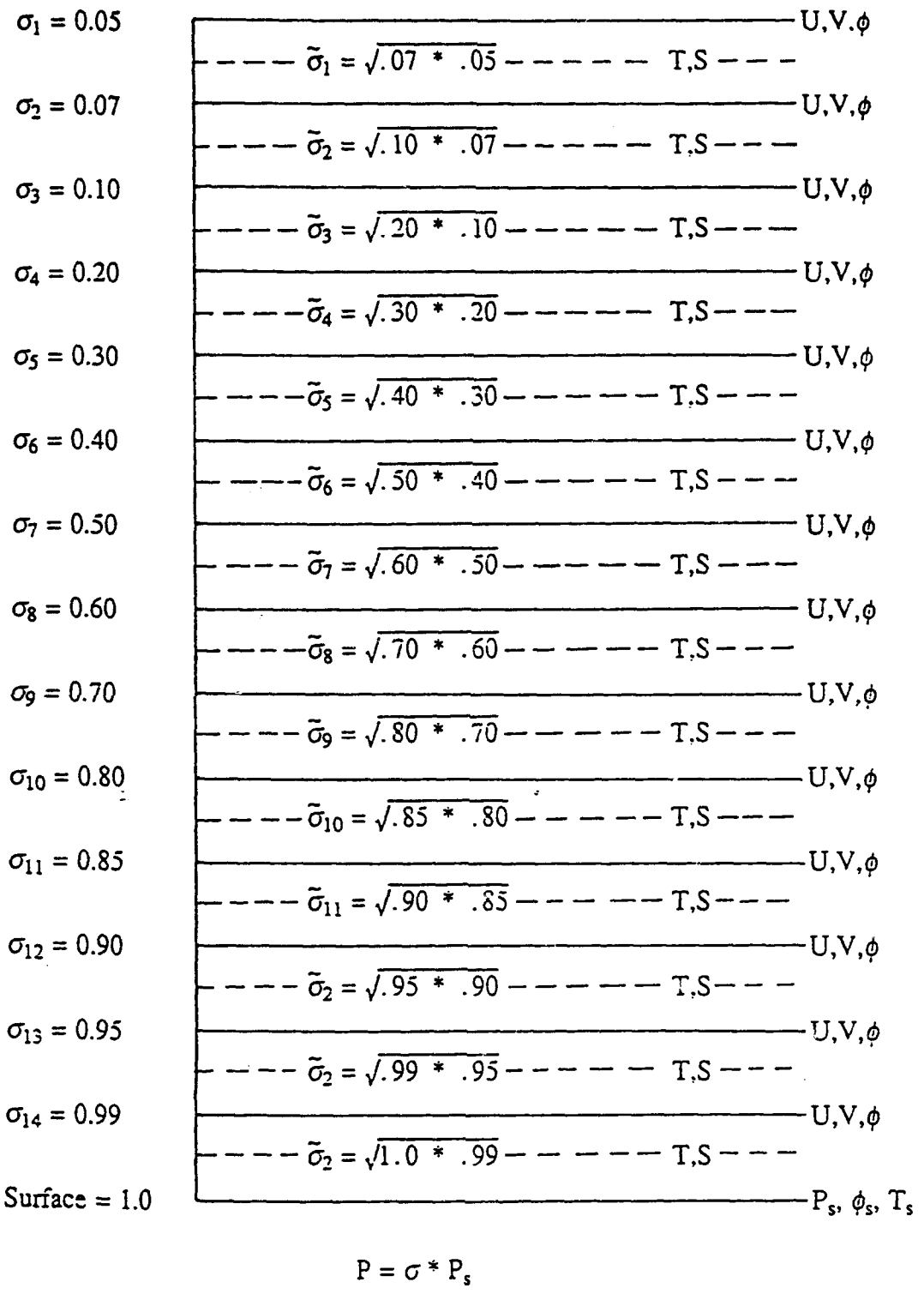

Figure 2.1 Schematic of FSUGSM vertical structure for 14 level version. All symbols have standard meteorological meaning except - S (dewpoint depression).

$CC_8 = N_L N_H (1 - N_M)$ low and high clouds

This sky condition is used in the computation of the solar radiation absorbed or scattered by clouds.

2.2.2 Deep cumulus convection

The deep cumulus convection of the FSUGSM follows Krishnamurti *et al.* (1993). The large scale supply of moisture I_L available for the clouds is defined by

$$I_L = -\frac{1}{g}\int_{p_b}^{p_t} \omega \frac{\partial q}{\partial p}\, dp \qquad (2.2)$$

where,

ω = large scale vertical velocity

q = large scale specific humidity

g = gravity

p_t = pressure at cloud top

p_b = pressure at cloud base

In this study an additional source of moisture is introduced to represent the mesoscale (subgrid - scale) moisture supply, $I_L \eta$. The total moisture supply I is then:

$$I = I_L (1 + \eta) \qquad (2.3)$$

Following Kuo (1974), the rainfall rate R and moistening rate M may be expressed as

$$R = I (1 - b) = I_L (1 + \eta) (1 - b) \qquad (2.4)$$

$$M = Ib = I_L (1 + \eta)\, b \tag{2.5}$$

where b is a moistening parameter.

Following Krishnamurti *et al.* (1983), the supply of moisture required to produce cloud over a unit area is as

$$Q = Q_q + Q_\theta \tag{2.6}$$

where

$$Q_q = \frac{1}{g}\int_{p_t}^{p_b} \frac{q_s - q}{\Delta\tau}\, dp \tag{2.7}$$

$$Q_\theta = \frac{1}{g}\int_{p_t}^{p_b} \left[\frac{C_p T(\theta_s - \theta)}{L\theta\Delta\tau} + \omega \frac{C_p T}{L\theta} \frac{\partial\theta}{\partial p} \right] dp \tag{2.8}$$

where L is latent heat of condensation, and C_p is specific heat of dry air at constant pressure. The Q_q term is the moisture required to change the environmental humidity distribution from q to q_s in a cloud time scale ($\Delta\tau$) of 30 minutes.

Two additional proportionality factors are now defined:

$$a_\theta = \frac{I(1 - b)}{Q_\theta} = \frac{I_L (1 + \eta)(1 - b)}{Q_\theta} \tag{2.9}$$

and

$$a_q = \frac{I\, b}{Q_q} = \frac{I_L(1 + \eta)b}{Q_q} \tag{2.10}$$

They may be related to the convective heating and moistening rate as:

$$\frac{\partial \theta}{\partial t} + V \cdot \nabla \theta = a_\theta \left[\frac{\theta_s - \theta}{\Delta \tau} + \omega \frac{\partial \theta}{\partial p} \right] \tag{2.11}$$

$$\frac{\partial q}{\partial t} + V \cdot \nabla q = a_q \frac{(q_s - q)}{\Delta \tau} \tag{2.12}$$

All of the variables to determine the convective heating and moistening rates are known from the large-scale, except η and b (a_θ and a_q are determined directly from equations (2.9) and (2.10) once η and b are known). Krishnamurti *et al.* (1983) determined η and b based on a screening multi-regression analysis of GATE observations. They regressed M/I_L and R/I_L against various large-scale variables such as vertical velocity, divergence, vertical shear of the horizontal wind, and vorticity. They found that the vertically averaged large-scale vertical velocity and the 700 mb relative vorticity provided the best estimates. The regression equations used were

$$\frac{M}{I_L} = a_1 \zeta_{700} + b_1 \overline{\omega} + c_1 \tag{2.13}$$

$$\frac{R}{I_L} = a_2 \zeta_{700} + b_2 \overline{\omega} + c_2 \tag{2.14}$$

where $a_1 = 1.58 \times 10^4$ sec, $b_1 = 3.04 \times 10^2$ sec/mb, $c_1 = 0.476$, $a_2 = 1.07 \times 10^4$ sec, $b_2 = 1.07 \times 10^2$ sec/mb, and $c_2 = 0.87$. These regression constants are used with the time dependent values of the vertically averaged vertical velocity and the 700 mb relative vorticity to produce time invarying values of the mesoscale moisture convergence and moistening parameters. They are computed from the following equations:

$$b = \frac{a_1 \zeta + b_1 \overline{\omega} + c_1}{(a_1 + a_2)\ \zeta + (b_1 + b_2)\ \overline{\omega} + (c_1 + c_2)} \tag{2.15}$$

and

$$\eta = [(a_1 + a_2)\ \zeta + (b_1 + b_2)\ \overline{\omega} + (c_1 + c_2)] - 1 \tag{2.16}$$

2.2.3 Shallow convection

Shallow convection in the FSUGSM follows the scheme of Tiedtke (1984) which assumes a simple diffusive form for the parameterization of shallow convection. Shallow convection is invoked for a conditionally unstable, undisturbed situation via K-theory. This parameterization scheme is used at points where the cloud base is below 700mb and the air is conditionally unstable. The cloud top may not extend above 700mb.

The moisture and the temperature equations for this parameterization are

$$\frac{\partial \overline{q}}{\partial t} = \frac{\partial}{\partial p} K_q \frac{\partial \overline{q}}{\partial p} \tag{2.17}$$

and

$$\frac{\partial \theta}{\partial t} = \frac{\partial}{\partial p} K_\theta \frac{\partial \theta}{\partial p} \tag{2.18}$$

where $K_q = K_\theta = Kg^2\rho^2$, K = 25 m^2/s, g is the gravity, and ρ is the density of air.

Krishnamurti *et al.* (1990) showed that a constant value of K does not produce a smooth continuity in the fluxes at the lifting condensation level (LCL). Instead, the following form of K was suggested

$$K_q = \frac{F_q(LCL)}{\rho^2 g \left[\frac{\partial \overline{q}}{\partial p} \right]_{LCL}} \tag{2.19}$$

where F_q (LCL) is the planetary boundary layer moisture flux at the LCL.

A similar definition of K_q was given for the same reason. This parameterization of shallow convection conserves moisture. The total convergence of moisture flux in the cloud layer equals F_q (LCL). These shallow clouds are nonprecipitating and do not produce saturation on the large scale.

2.3 Explicit cloud scheme

Explicit cloud scheme adopted in FSUGSM follows Mannoji (1993).

The basic equations for the local change in the cloud water mixing ratio (m) and the cloud cover (f) prediction, respectively, are

$$\frac{\partial m}{\partial t} = \frac{\partial m_{ST}}{\partial t} + \frac{\partial m_{CV}}{\partial t} + \frac{\partial m_{PP}}{\partial t} + \frac{\partial m_{EC}}{\partial t} \tag{2.20}$$

$$\frac{\partial f}{\partial t} = \frac{\partial f_{ST}}{\partial t} + \frac{\partial f_{CV}}{\partial t} + \frac{\partial f_{PP}}{\partial t} + \frac{\partial f_{EC}}{\partial t} \tag{2.21}$$

where subscripts ST, CV, PP, and EC denote stratiform cloud, convective cloud, precipitation, and evaporation of cloud, respectively.

The temperature and moisture equations can then be expressed by

$$\frac{dT}{dt} = A(T) - \frac{L}{C_p}\left[\frac{\partial q_{ST}}{\partial t} + \frac{\partial q_{EC}}{\partial t} + \frac{\partial q_{ER}}{\partial t}\right] \tag{2.22}$$

$$\frac{dq}{dt} = A(q) + \left[\frac{\partial q_{ST}}{\partial t} + \frac{\partial q_{EC}}{\partial t} + \frac{\partial q_{ER}}{\partial t}\right] \tag{2.23}$$

where A(T) and A(q) represent change in temperature and moisture respectively. These changes are produced by processes that are not associated with the explicit cloud scheme such as advection, and turbulence, etc. Subscript ER denotes evaporation of rain. In practice note that $\frac{\partial q_{ST}}{\partial t} = - \frac{\partial m_{ST}}{\partial t}$ and $\frac{\partial q_{EC}}{\partial t} = - \frac{\partial m_{EC}}{\partial t}$.

The overall processes of the explicit cloud scheme are schematically illustrated in Figure 2.2.

2.3.1 Stratiform clouds

Following Sundqvist (1978), the formation and dissipation of stratiform clouds are calculated from changes in temperature and moisture due to non-convective processes. Unlike Sundqvist's scheme in which cloud cover is diagnostically calculated from relative humidity, this scheme predicts cloud cover.

In the computation of the rate of change of cloud water and cloud cover it is assumed that

1) over the grid box the temperature distribution is uniform and thus the saturated humidity field is also uniform,
2) in the overcast area $q = q_s$ and in the open area q is evenly distributed between a minimum value and q_s,
3) cloud water is uniformly distributed between zero and a maximum value over the overcast area,
4) changes of T and q are uniform, and
5) cloud forms when the relative humidity exceeds the critical values. The above mentioned assumptions are applied in a single grid box. We note that the minimum value of moisture and the maximum value of cloud water should be derived from known model variables.

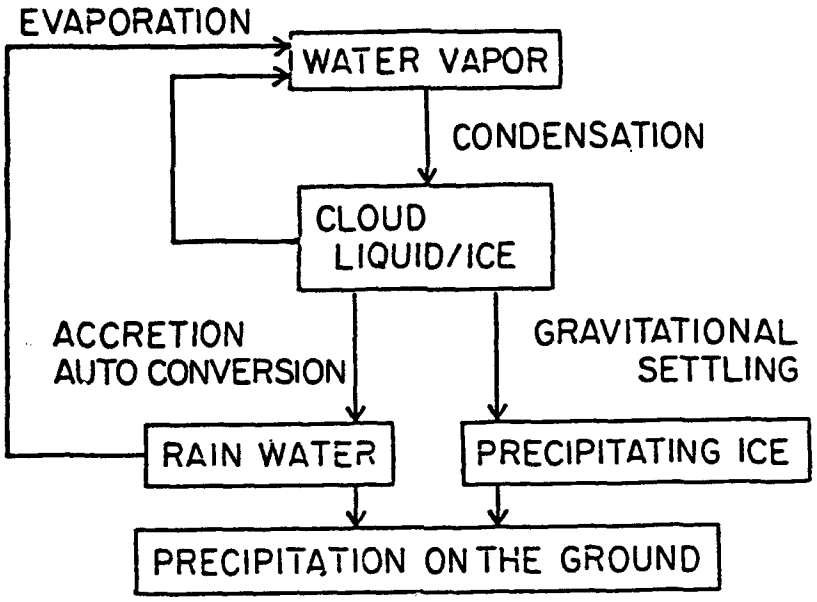

Figure 2.2 Overall process adopted in the FSUGSM explicit cloud scheme.

To close the parameterization of the cloud water and cloud cover a relationship between the cloud variables and the large-scale variables needs to be prescribed. According to Mannoji (1993) this relationship is

$$\Delta q_s - \frac{\varepsilon L^2 q_s}{RC_pT^2}\Delta m = -\frac{q_s}{p}\delta p + \frac{\varepsilon L q_s}{RT^2}\delta T \tag{2.24}$$

or

$$\delta q - \Delta q_s = M - \gamma\Delta m \tag{2.25}$$

where

$$M = \delta q + \frac{q_s}{p}\delta p - \frac{\varepsilon L q_s}{RT^2}\delta T \tag{2.26}$$

and

$$\gamma = \frac{\varepsilon L^2 q_s}{RC_pT^2} \tag{2.27}$$

In equation (2.24) Δq_s and Δm denote, respectively, change in the cloud saturated humidity and the cloud water while δq, δp, and δT denote changes in large-scale variables, q, p, and T, respectively. These large-scale changes are known. The saturated humidity, q_s, is also a known large-scale model variable. R is gas constant and ε is equal to 0.622.

Stratiform cloud processes consist of two processes: formation and dissipation. Equation (2.24) is used to find solutions for each process. Defining Δf to be change in the cloud cover, Mannoji (1993) proposed a closure for Δm and Δf based on a geometric method as illustrated in Figures 2.3 and 2.4 for the formation and dissipation processes, respectively.

Formation process

Figure 2.3 illustrates that when water vapor increases or temperature decreases (that is, M is greater than 0) water vapor condenses, and thus it turns into cloud water if saturated, while q_s may increase by $\tau\Delta q_s$ due to temperature change. This means that condensation occurs when specific humidity exceeds $q_s + \tau\Delta q_s$.

From Figure 2.3 the equations for Δm and Δf are readily obtained as

$$\Delta m = (\delta q - \Delta q_s)(f + \frac{\tau}{2}\Delta f) \tag{2.28}$$

and

$$\Delta f = (\delta q - \Delta q_s)\frac{1 - f}{q_s - q_{min}} \tag{2.29}$$

where q_{min} can be represented by the known variables as

$$q_s f + \frac{q_{min} + q_s}{2}(1 - f) = q \tag{2.30}$$

or

$$q_{min} = \frac{2(q - q_s f)}{1 - f} - q_s \tag{2.31}$$

This formulation ensures that q_{min} is consistent with both the moisture in the grid box and its saturated value.

Using equations (2.25), (2.28), and (2.29), the solutions for Δf and Δm are

$$\Delta m = \frac{1}{2\gamma^2\lambda}\left[\gamma(f+M\lambda) + M\gamma + 1 - \sqrt{\{\gamma(f+2M\lambda)+1\}^2 - 4\gamma^2 M\lambda(f+M\lambda)}\right] \tag{2.32}$$

and

$$\Delta f = \frac{(M - \gamma\Delta M)(1 - f)^2}{2(q_s - q)} \tag{2.33}$$

where

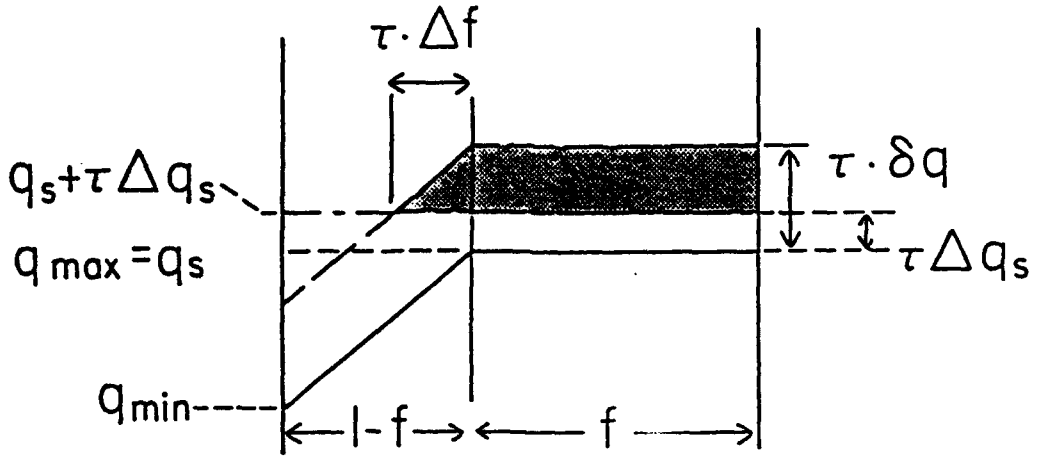

Figure 2.3 Distribution of the water vapor and cloud cover within a grid during the stratiform cloud formation. Water vapor distributions before (solid line) and after (dashed line) condensation occurs are shown. Amount of the cloud water condensed at one time-step is shaded.

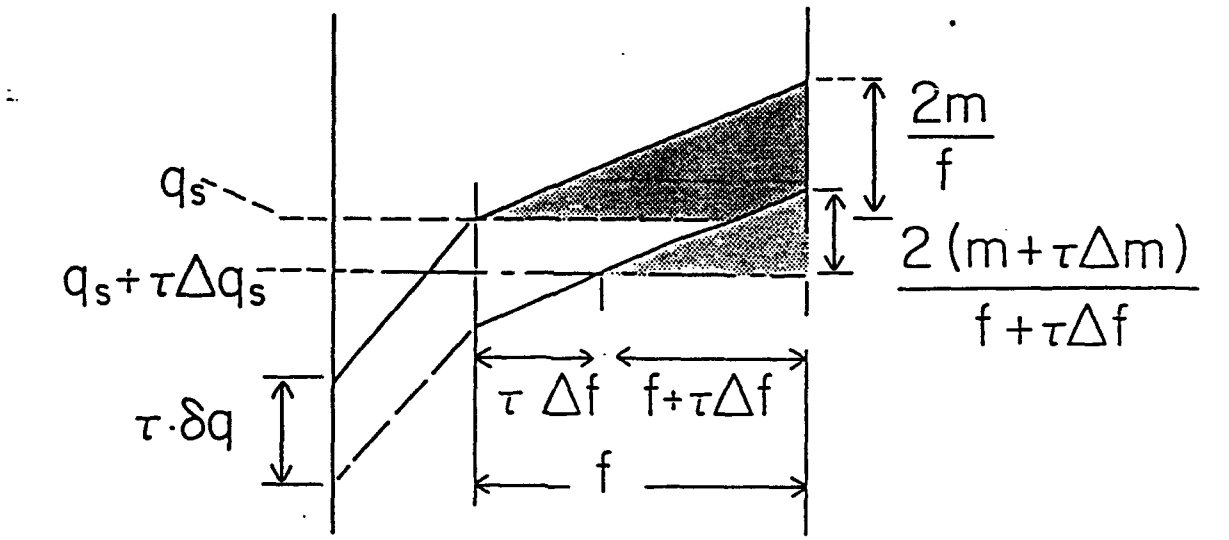

Figure 2.4 Distribution of the water vapor, cloud water and cloud cover in a grid during the stratiform cloud dissipation. Shades show cloud water amount before (heavily) and after (lightly) dissipation occurs.

$$\lambda = \frac{\tau(1 - f)^2}{4(q_s - q)} \tag{2.34}$$

Given the large scale variations δp, δq, and δT, Δm and Δf can readily be calculated.

Dissipation Process

Mannoji (1993) again utilizes the geometric method to achieve the closure of the dissipation process in a manner similar to that used for the formation process.

Figure 2.4 shows that when water vapor decreases or temperature increases (i.e. M is smaller than zero) cloud water evaporates and thus it turns into water vapor if unsaturated, while q_s may decrease by $\tau\Delta q_s$ due to temperature change. Evaporation, therefore, occurs when specific humidity becomes less than $q_s + \tau\Delta q_s$ where Δq_s is negative.

The equations for a closure of Δf and Δm are then given by

$$\frac{\Delta f}{\delta q - \Delta q_s} = \frac{f}{2m/f} \tag{2.35}$$

and

$$\frac{2(m+\tau\Delta m) \;/\; (f+\tau\Delta f)}{f + \tau\Delta f} = \frac{2m/f}{f} \tag{2.36}$$

where 2m/f represents a maximum value of cloud water. Equation (2.36) can be written as

$$\Delta m = \frac{m\Delta f}{f}\left(2 + \frac{q\Delta f}{f}\right) \tag{2.37}$$

Note that when $\tau\Delta f/f$ equals -1, the cloud disappears. This means that cloud cover and

cloud water becomes zero and Δm becomes equal to $m\Delta f/f$ from equation (2.37).

With the aid of equations (2.25), (2.35) and (2.37), the solution for Δf is

$$\Delta f = \frac{1}{\tau\gamma}\left[-(1+\gamma f) + \sqrt{(1+\gamma f)^2 + \frac{\tau\gamma f^2 M}{m}}\right] \tag{2.38}$$

Once Δf is determined, Δm is calculated from equation (2.37).

2.3.2 Convective clouds

Total condensation in a column and time tendency of T and q at each level are computed by the FSUGSM cumulus convection scheme described earlier. Two assumptions are required to calculate the cloud water source. These assumptions are:

1) The total condensation in the column, P, represents the vertically integrated cloud water source and is given by

$$P = \frac{1}{g}\int_0^{p_s} \frac{\partial m_{cv}}{\partial t}\, dp \tag{2.39}$$

This is based on conservation of mass of water in the column.

2) The amount of cloud water at each level is proportional to a vertical distribution function, D, which is arbitrarily chosen to have a linear variation from 1 at the cloud base to 0.4 at the cloud top. Here, cloud top and cloud base are provided by the implicit cumulus convection scheme.

For a complete closure of the convective cloud cover formation, the cloud cover

is determined following Le Treut (1990). He assumes that the uniformly distributed total water within the grid box is split into a vapor part and a liquid part, provided that the total water and its maximum and minimum values are given. This is best illustrated in Figure 2.5.

The closure equation obtained from Figure 2.5 is:

$$\frac{2m/f}{f} = \frac{q_s - q_{min}}{1 - f} \tag{2.40}$$

Combining equations (2.31) and (2.40), the equation for the cloud cover due to the convective cloud formation process is given by

$$f_{cv} = \frac{1}{1 + \sqrt{\frac{q_s - q}{m}}} \tag{2.41}$$

Assuming that the cloud cover becomes f_{cv} when f_{cv} is greater than the cloud cover at the previous time step, f(t - 1), the equation can be written by

$$\frac{\partial f_{cv}}{\partial t} = \begin{cases} \frac{f_{cv} - f(t-1)}{\tau} & \text{if } f_{cv} > f(t-1) \\ 0 & \text{if } f_{cv} \le f(t-1) \end{cases} \tag{2.42}$$

2.3.3 Precipitation

Mannoji (1993) used the Sundqvist scheme to calculate the conversion of cloud water to raindrops, cloud ice sedimentation, evaporation of raindrops, and the rate of change of cloud water and precipitation fluxes.

Since the model does not separate cloud ice and cloud liquid water, the

proportion of cloud liquid water needs to be prescribed. Following Sundqvist (1989), this is diagnostically prescribed as:

$$R = \begin{cases} 0 & \text{for } T < T_1 \\ -2\left[\frac{T-T_1}{T_2-T_1}\right]^3 + 3\left[\frac{T-T_1}{T_2-T_1}\right]^2 & \text{for } T_1 \le T < T_2 \\ 1 & \text{for } T \ge T_2 \end{cases} \qquad (2.43)$$

where T_1 and T_2 are taken to be 233 K and 273 K, respectively. These are used for a smooth transition between frozen and liquid states. Cloud in the precipitation process is divided into two parts. One part is liquid cloud in which liquid water content is given by Rm and cloud cover by Rf. The other part involves cloud ice in which ice content is represented by (1 - R)m and cloud cover by (1 - R)f. Therefore, the ratio of cloud water to ice content does not change in the overcast area.

Cloud to raindrops

Following Sundqvist (1989), the conversion rate of cloud water to rain, P_{liq}, is given by

$$P_{liq} = C_t m \left\{ 1 - \exp\left[-\left[\frac{m/f}{m_c} \right]^2 \right] \right\} \qquad (2.44)$$

where C_t denotes the time constant, m_c a critical cloud water. In practice, this equation is modified by Sundqvist (1989) as

$$P_{liq} = C_t R\,(m - f m_c F)\,F \qquad (2.45)$$

where

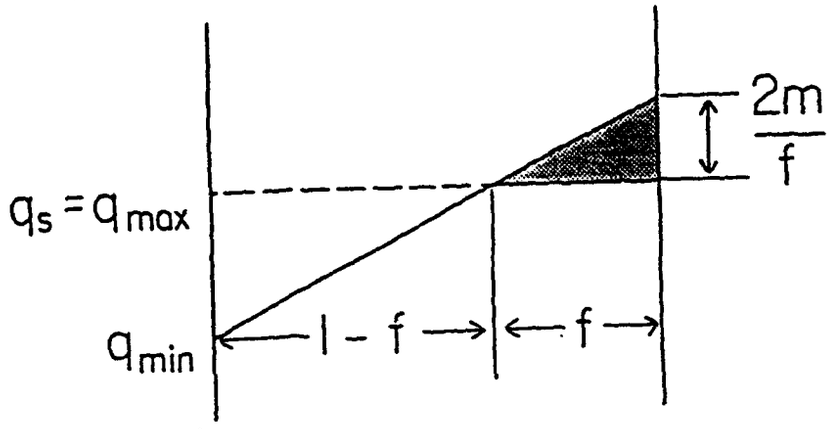

Figure 2.5 Distribution of the water vapor and cloud water to determine the cloud cover of cumulus cloud in a grid. Amount of the cloud water is shaded.

$$F = 1 - \exp\left[-\left(\frac{m / f}{m_c}\right)^2\right] \tag{2.46}$$

$$C_t = C_o (1 + C_1\sqrt{P_r}) \{1 + C_2 \sqrt{(268 - T)}\} \tag{2.47}$$

$$m_c = m_o / [(1 + C_1\sqrt{P_r}) \{1 + C_2 \sqrt{(268 - T)}\}] \tag{2.48}$$

where C_0, C_1, C_2, and m_0 are constants listed in Table 2.1, and P_r denotes the rate of precipitation which will be shown in the next section.

Table 2.1: Parameters used in parameterization of precipitation. (stratus/cumulus cloud for C_0 and m_0)

C_0	10^{-3} / 10^{-4}	s^{-1}
m_0	5×10^{-4} / 3×10^{-4}	kg/kg
C_1	300	$(kg\ m^{-2}\ s^{-1})^{-1/2}$
C_2	0.5	$K^{-1/2}$

Cloud ice sedimentation

The rate of change in cloud ice due to flux divergence is expressed as

$$S = g \frac{\partial F_i}{\partial p} \tag{2.49}$$

where the flux divergence of cloud ice is given by

$$F_i = (1 - R)\, f(\rho_a\, m_i\, v) \tag{2.50}$$

where ρ_a is the density of air, m_i is cloud ice mixing ratio, and v is the fall speed of cloud ice.

Unlike cloud liquid water, the fall speed of cloud ice is not negligible. Heymsfield (1977) formulated the fall speed of ice from observations as

$$v = 3.326\, (\rho m_i)^{0.17} \tag{2.51}$$

The conversion rate of cloud ice to precipitation due to sedimentation process can then be expressed as

$$P_i = \begin{cases} S & \text{for } S > 0 \\ 0 & \text{for } S \le 0 \end{cases} \tag{2.52}$$

Finally the rate of change of cloud cover due to precipitation is given by

$$\frac{\partial f_{pp}}{\partial t} = \begin{cases} (1\text{-}R)f/\tau & \text{if } P_i\tau > (1\text{-}R)m \\ 0 & \text{if } P_i\tau < (1\text{-}R)m \end{cases} \tag{2.53}$$

Evaporation of raindrops

The equation for evaporation of raindrops is expressed in Sundqvist (1989) as

$$\frac{\partial q_{ER}}{\partial t} = \frac{K_{ER}\ (1-f)\ (1-RH)}{\sqrt{P_r}} \tag{2.54}$$

where K_{ER} is raindrop evaporation constant, which is taken to be 10^{-5} (kg $m^{-2}s)^{-1/2}$.

Rate of change of cloud water and precipitation flux

The rate of change of cloud water is computed from

$$\frac{\partial m_{RE}}{\partial t} = S - P_{liq} - P_i \tag{2.55}$$

and the flux of precipitation is given by the equation

$$P_r = \frac{1}{g}\int_0^p \left[P_{liq} + P_i - \frac{\partial q_{ER}}{\partial t} \right] dp \tag{2.56}$$

Therefore, total precipitation on the ground, P, is

$$P = P_r + F_i \tag{2.57}$$

2.3.4 Evaporation of cloud

Evaporation of cloud is accelerated by the turbulent mixing between cloud air and unsaturated environment air. This is taken into account in the cloud dissipation process (Tiedtke, 1991) as

$$\frac{\partial m_{EC}}{\partial t} = - K_{EC}\, f(q_s - q) \tag{2.58}$$

$$\frac{\partial f_{EC}}{\partial t} = \frac{\partial m_{EC}}{\partial t}\left(\frac{f}{m}\right) \tag{2.59}$$

where cloud evaporation constant, K_{EC}, is equal to $10^{-6}s^{-1}$.

2.3.5 Radiation for cloud liquid and ice

The predicted cloud water content is employed in radiation scheme to calculate the optical depth and emissivity. Emissivity is computed in the infrared and shortwave regions.

In the infrared region, the emission function is computed from the expression:

$$\varepsilon_{IR} = 1 - \exp(-kW) \tag{2.60}$$

where k and W denote the absorption coefficient and the cloud water path, respectively. The absorption coefficient is taken to be 0.14 for cloud liquid and 0.05 for cloud ice (Stephens, 1978; Starr and Cox, 1985).

In the shortwave region, the emission function is calculated from the equation given by Platt and Harshvardhan (1988):

$$\varepsilon_{IR} = 1 - \exp(-0.757\ \tau_{SW}) \tag{2.61}$$

where τ_{SW} represents the optical depth in the shortwave region. Stephens (1978) expressed the optical depth for cloud liquid as

$$\tau_{SW} = \exp\{\ 0.606 + 3.94 \log(\log W)\ \} \tag{2.62}$$

and for cloud ice as

$$\tau_{sw} = 93.409\ W \tag{2.63}$$

2.3.6 Initial condition and computational procedure

Initial values of the cloud variables are based on the procedure given by Pudykiewicz *et al.* (1992). Initially, the mean relative humidity ($\overline{RH}$) is taken to be the relative humidity at each pressure level in the column. Given this humidity field, the cloud cover is diagnosed from equation (2.1). The cloud water content (CWC) is initially assigned as

$$CWC = 10^{\left(\frac{T-273}{20} - 4\right)} \quad \text{in Kg/m}^3 \tag{2.64}$$

Here, the maximum value of cloud water content is limited to 5×10^{-5} Kg/m^3.

To avoid unrealistic fall-outs of condensation, discretion in computational procedure is advised. The sequence of processes adopted in the explicit cloud parameterization scheme of FSUGSM is as follows: 1) convective cloud formation, 2) stratiform cloud formation and dissipation, 3) removal of supersaturation, 4) precipitation process and raindrop evaporation, and 5) evaporation of cloud by turbulent mixing.

The temperature and moisture changes, δT and δq, are computed using the large-scale parameters. δq is obtained by adding all changes in moisture due to vertical advection, turbulent transfer, and adjustment. δT is calculated in a similar way, but with the inclusion of changes in temperature due to radiative transfer.

Adjustment scheme in the FSUGSM explicit cloud scheme is described in Betts

(1973) and Smith (1990). During the changing state of cloud water, the liquid water temperature, T_{liq}, and the total water content, q_t, are conserved. These are defined as

$$T_{liq} = T - \frac{L}{Cp} m \tag{2.65}$$

and

$$q_t = q + m \tag{2.66}$$

In the unstable layers the lapse rate of T_{liq}, Γ_ℓ, is set equal to the dry adiabatic lapse rate, Γ_d. The change in the total water content is calculated in those layers in which the lapse rate has been changed to Γ_d. Since the total water content is conserved, the change of total water should be set to be zero. Temperature and moisture changed by the adjustment process are used in the stratiform cloud process to calculate condensation and/or evaporation.

2.4 Radiation

The radiation parameterization of the FSUGSM consists of the parameterization of the short-wave and long-wave radiation. These are briefly described in the following sections.

2.4.1 Short-wave radiation

The short-wave radiation parameterization of the FSUGSM is based on the scheme of the UCLA/GLAS GCM as described by Davies (1982) and Harshvardhan *et al.* (1987). It includes a parameterization for the major absorption processes in the stratosphere, the troposphere, and at the earth's surface. The parameterization utilizes the water vapor distribution, the cloud coverage, the zenith angle of the sun, the albedo

of the earth's surface, and the ozone distribution.

In this scheme multiple scattering is taken into account. Following is a brief description of the short-wave radiation parameterization. The heating rate at pressure level p due to the short-wave radiative flux is given by

$$\frac{dT}{dt} = \frac{g}{C_p} \frac{d}{dp} (S^{\uparrow}(p) - S(p)^{\downarrow}) \tag{2.67}$$

where $S^{\downarrow}(p)$ is the downward solar radiative flux at pressure level p, and $S^{\uparrow}(p)$ is the upward solar radiative flux at p by reflection from layers below p and the ground.

2.4.1.1 Basic equation for transfer of shortwave radiation

The basic equations for the downward and upward solar flux at pressure p for a nonscattering atmosphere are, respectively:

$$S^{\downarrow}(p) = \mu_0 S_0 \tau(u(p)) \tag{2.68}$$

$$S^{\uparrow}(p) = \mu_0 S_0 R_g \tau(u(p)^*) \tag{2.69}$$

where

μ_0 = cosine of the zenith angle (θ_0)

S_0 = net solar radiation at the top of the atmosphere

R_g = surface albedo integrated over the entire solar spectrum

$\tau(u(p))$ = mean transmittance integrated over the entire solar spectrum

u = optical path for the absorber

u^* = effective optical path traversed by the diffusively reflected radiation

$$= Mu_0 + (u_0 - u) \overline{M} \tag{2.70}$$

where

u_0 = total optical path up to the ground

$\overline{M}$ = effective magnification factor for diffuse radiation

The definition of $\tau(u)$ is given by

$$\tau(u) = \frac{1}{\Delta\nu}\int_{\Delta\nu} \exp\left[- M \int_{p}^{0} k_{\nu}\, du\right] d\nu \qquad (2.71)$$

where

ν = spectral wavenumber

$\Delta\nu$ = spectral width

M = magnification factor accounting for the slant path and refraction which is given by

$$M = \frac{35}{(1224\ \mu_0^2 + 1)} \qquad (2.72)$$

k_{ν} = monochromatic mass absorption coefficient

Different atmospheric constituents (water vapor, O_3, etc.) have different absorption properties. Since the heating rate by the short-wave radiation can be expressed in terms of absorption functions, it is important to determine the absorption functions.

2.4.1.2 Water vapor absorption

Absorption by water vapor is the major source of solar radiative heating in the atmosphere (Lacis and Hansen, 1974). For clear skies the absorption due to water

vapor is modeled based on the k-distribution approximation (Stephens, 1984) in which the absorptivity, $A_{wv}(y)$, is expressed as

$$A_{wv}(y) = 1 - \int_0^{\infty} p(k)\, e^{-ky}\, dk \tag{2.73}$$

where,

$p(k)$ = probability distribution for the absorption coefficient

$p(k)dk$ = fraction of the incident flux that is associated with an absorption coefficient between k and k + dk

y = effective optical depth of water vapor

The effective optical depth of water vapor is given by

$$y = \frac{M(\mu)}{g} \int_0^{p_s} q \left(\frac{p}{p_0}\right)\left(\frac{T_0}{T}\right)^{\frac{1}{2}} dp \tag{2.74}$$

where,

M = magnification factor

g = gravity

q = specific humidity

p_0 = reference pressure = 1013.25 mb

T_0 = reference temperature = 273.16 K

For the upward beam in a clear sky, the effective optical depth is given by

$$y^* = \frac{M(\mu)}{g}\int_0^{p_s} q\left(\frac{p}{p_0}\right)\left(\frac{T_0}{T}\right)^{\frac{1}{2}}\,dp + \frac{\sqrt{3}}{g}\int_p^{p_s} q\left(\frac{p}{p_0}\right)\left(\frac{T_0}{T}\right)^{\frac{1}{2}}\,dp \qquad (2.75)$$

The net absorption by water vapor in a clear sky in the i^{th} layer is then:

$$A_{iwv} = \mu_0 S_0 \left\{A_{wv}(y_{i+1}) - A_{wv}(y_i) + R_g(\mu)\,[A_{wv}(y^*_{i+1})]\right\} \qquad (2.76)$$

where

S_0 = solar flux at the top of the atmosphere

$R_g(\mu)$ = ground albedo

For cloudy skies multiple scattering is the principal factor affecting the absorption by water vapor. The parameterization of cloudy sky water vapor absorption is also based on the discrete probability distribution which is the k-distribution method. The complete radiative transfer problem including multiple scattering is solved as discussed by Davies (1982). Apart from the absorption, the reflection and transmission characteristics of each atmospheric layer need to be determined, given the total optical thickness δ, the single scattering albedo $\tilde{\omega}$, the asymmetry scattering factor $\tilde{g}$, and the solar zenith angle θ. The solution is done through a two-stream approximation. From among the various two-stream approximation available, the delta-Eddington approximation given by Joseph (1976) is used. In this approximation, the transfer of the direct solar beam radiation through a single homogeneous layer is assumed to give rise to a diffuse radiation at the top of the layer (the reflected part, UO) and a diffuse radiation at the bottom of the layer (the transmitted part, DO). The upward diffuse radiation UO and the downward diffuse radiation DO are given as a function of δ', $\tilde{\omega}'$ and $\tilde{g}'$ where

$$\delta' = \delta(1 - \tilde{g}^2\tilde{\omega}) \tag{2.77}$$

$$\tilde{\omega}' = \tilde{\omega}(1 - \tilde{g}^2) / (1 - \tilde{g}^2\tilde{\omega}) \tag{2.78}$$

$$\tilde{g}' = \tilde{g} / (1 + \tilde{g}) \tag{2.79}$$

All these parameters were transformed based on the asymmetry factor ($\tilde{g}$) to normalize the delta-Eddington phase function. The reflection R and transmission T functions for each homogeneous layer are approximated by the two-stream approximation of Sagan and Pollack (1967):

$$R = \frac{(u+1)(u-1)(e^t - e^{-t})}{(u+1)^2e^t - (u-1)^2e^{-t}} \tag{2.80}$$

$$T = \frac{4u}{(u+1)^2e^t - (u-1)^2e^{-t}} \tag{2.81}$$

where

$$u = \left[\frac{1 - \tilde{g}\tilde{\omega}}{1 - \tilde{\omega}}\right]^{\frac{1}{2}} \tag{2.82}$$

$$t = [3(1 - \tilde{\omega})(1 - \tilde{g}\tilde{\omega})]^{\frac{1}{2}}\,\delta \tag{2.83}$$

Using these equations, the reflection and transmission functions and the upwelling and downwelling radiation due to the direct solar beam can be calculated at all levels.

The direct-beam radiation reflected and transmitted by a layer may be considered as sources of diffuse radiation for the layers above and below it. The upwelling and downwelling radiation at each layer, as given by Harshvardhan *et al.* (1987), is:

$$UO_i = \mu_0 S_i R_i(\mu_0) \qquad i = 1, \ldots, n+1 \tag{2.84}$$

$$DO_i = \mu_0 S_i T_i(\mu_0) \qquad i = 1, \ldots, n \tag{2.85}$$

where

UO_i = upwelling radiation through level i

DO_i = downwelling radiation through level i

R_i = reflectivity of layer i to unit diffuse radiation

T_i = transmissivity of layer i to unit diffuse radiation

$\mu_0 S_i$ = direct solar flux incident on level i

The downwelling diffuse radiation at level i+1 due to all diffuse radiation that has not crossed level i is

$$D1_i = (D1_i + UO_i\, CR_i)\, M_i T_i + DO_i \qquad i = 1, \ldots, n+1 \tag{2.86}$$

where

CR_i = composite reflection coefficient of the atmosphere above i

M_i = magnification factor for multiple reflections

Here, CR_i is recursively obtained by

$$CR_i = R_{i-1} + T_{i-1}\, CR_{i-1}\, T_{i-1}\, M_{i-1} \qquad i = 2, \ldots, n+1 \tag{2.87}$$

M_i is given by

$$M_i = 1 / (1 - CR_i R_i) \qquad i = 1, \ldots, n+1 \tag{2.88}$$

By definition

$$CR_1 = 0 \quad \text{and} \quad DO_1 = 0 \tag{2.89}$$

The upwelling diffuse radiation at i due to all diffuse radiation that has not previously crossed level i+1 is

$$U1_i = (D1_i R_i + UO_i)\, M_i \qquad i = 1, \ldots, n+1 \tag{2.90}$$

Once $D1_i$ and $U1_i$ are found for all i, the total radiation crossing each level may be recursively calculated by

$$U_i = U1_i + U_{i+1}\, T_i\, M_i \qquad i = n, \ldots, 1 \tag{2.91}$$

$$D_i = D1_i + U_i\, CR_i + \mu_0 S_i \qquad i = n+1, \ldots, 1 \tag{2.92}$$

To obtain the broadband values, each of the spectral values calculated above are summed. The absorbed radiation within each layer is then found directly from the net flux convergence of solar radiation.

2.4.1.3 Ozone absorption

According to Lacis and Hansen (1974) the major source of stratospheric heating is the absorption of solar radiation by ozone. The absorption due to ozone occurs at wavelengths where Rayleigh scattering is significant. Most of the Rayleigh scattering takes place below the ozone layer, so the lower atmosphere acts mainly as a reflecting layer.

The absorption due to ozone is different in the weak visible bands (Chapius band) versus the ultraviolet bands (Hartley and Huggins bands). The percentage of solar flux absorbed as function of ozone amount for the two spectral regions are given in Lacis and Hansen (1974). They showed that the ultraviolet bands are practically saturated at 0.5 cm of ozone, while absorption in the visible bands remain nearly proportional to the ozone amount. The total fractional absorption is expressed as

$$A(X) = A_{uv}(X) + A_{vis}(X) \tag{2.93}$$

where X is effective ozone amount in cm (STP), $A_{uv}(X)$ is the fraction of incident solar flux that is absorbed in the ultraviolet bands, and $A_{vis}(X)$ is the fraction of incident solar flux that is absorbed in the visible bands.

Lacis and Hansen (1974) fitted the frequency-integrated absorption curves for ozone to analytical expressions:

$$A_{uv}(X) = \frac{1.082X}{(1+138.6X)^{0.805}} + \frac{0.0658X}{1 + (103.6X)^3} \tag{2.94}$$

$$A_{vis}(X) = \frac{0.02118X}{1 + 0.042X + 0.000323X^2} \tag{2.95}$$

The ozone amount traversed by the direct solar beam in reaching the i^{th} layer of the atmosphere is

$$X_i = u_i M \tag{2.96}$$

where

u_i = amount of ozone in a vertical column above the i^{th} layer

M = magnification factor accounting for the slant path and refraction

The ozone path traversed by the diffuse radiation illuminating the i^{th} layer from below is

$$X_i^* = u_t M + 1.9(u_t - u_i) \tag{2.97}$$

where u_t is the total ozone amount in a vertical path above the main reflecting layer (which is the ground for clear skies or the cloud top for cloudy skies). The total absorption of short-wave radiation in the i^{th} layer due to ozone is then:

$$A_i = \mu_0 S_0 \left\{A(X_{i+1}) - A(X_i)\right\} + \mu_0 S_0 \bar{R}(\mu_0) \left\{A(X_i^*) - A(X_{i+1}^*)\right\} \tag{2.98}$$

where $\bar{R}(\mu_0)$ is the albedo of the reflecting region including the effective albedo of the lower atmosphere and the ground reflectivity.

2.4.1.4 Earth's surface absorption

The surface absorption is divided into two parts. One portion concerns the wavelength regions where the absorption coefficient of water vapor is significant. The other part covers absorption in the remaining wavelengths. Therefore, the total surface absorption is the sum of the absorption in the spectral regions associated with significant water vapor absorption and the spectral regions of negligible water absorption. That is

$$A_g = A_{g1} + A_{g2} \tag{2.99}$$

where

A_g = total surface absorption

A_{g1} = surface absorption in the spectral region associated with significant water vapor absorption (calculated differently for clear and cloudy skies)

A_{g2} = surface absorption in the spectral regions of negligible water vapor absorption

For clear skies,

$$A_{g1} = \mu_0 S_0 [1 - R_g(\mu_0)] \int_0^{\infty} p(k) e^{-ky} \, dk \tag{2.100}$$

$$A_{g2} = \mu_0 S_0 [1 - \bar{R}_G(\mu_0)][0.647 - A(u_t M)] \tag{2.101}$$

where

R_g = ground albedo

$\bar{R}_G$ = albedo of the ground and the atmosphere above

For cloudy skies, A_{g1} is obtained by multiplying the transmission function at the ground by $[1 - \bar{R}_g(\mu_0)]$. A_{g2} is computed using equation (2.99), where $\bar{R}_G(\mu_0)$ is obtained accounting for the optical depth for clouds, δ_c, and the asymmetry scattering factor for clouds, $\tilde{g}_c$.

2.4.2 Long-wave radiation

The long-wave radiation scheme of the model is also based on the UCLA/GLAS GCM scheme and is described by Harshvardhan and Corsetti (1984). It includes a

parameterization of the transmission functions for carbon dioxide and water vapor using the band-wing scaling approximation developed by Chou and Peng (1983) and Chou (1984). It also includes the computation of the transmission functions for ozone based on the formulation given by Rodgers (1968).

The radiative cooling rate due to the long-wave radiative flux is given by

$$\frac{dT}{dt} = -\frac{g}{Cp} \frac{d\,(F\downarrow(p) - F\uparrow(p))}{dp} \tag{2.102}$$

where $F\downarrow(p)$ and $F\uparrow(p)$ are the long-wave downward and upward fluxes at pressure level p, respectively. This is the final output of the radiation scheme.

2.4.2.1 Basic equation for transfer of longwave radiation

The basic equations for the clear-sky longwave downward ($F^{\downarrow}_{clr}$) and upward ($F^{\uparrow}_{clr}$) fluxes integrated over the spectral range $\Delta\nu$ are

$$F^{\downarrow}_{clr}(p) = \int_{\Delta\nu}\left[\int_{p_t}^{p} B_\nu(T(p')) \frac{d\tau_\nu(p,p')}{dp'} dp'\right] d\nu \tag{2.103}$$

$$F^{\uparrow}_{clr}(p) = \int_{\Delta\nu}\left[B_\nu(T_s)\,\tau_\nu(p,p_s) + \int_{p_s}^{p} B_\nu(T(p') \frac{d\tau_\nu(p,p')}{dp'} dp'\right] d\nu \tag{2.104}$$

where

$B_\nu(T_s)$ = blackbody flux at the surface temperature T_s

p_s = pressure at the bottom of the atmosphere

p_t = pressure at the top of the atmosphere

$T(p')$ = air temperature at pressure p'

$\tau_\nu(p,p')$ = diffuse transmittance between levels p and p′

Integrating by parts above equations (2.103) and (2.104) gives

$$F^{\downarrow}_{clr}(p) = B(T(p)) - G(p,p_t,T(p_t)) + \int_{T(p)}^{T(p_t)} \frac{\partial G(p,p',T(p'))}{\partial T}\, dT(p') \qquad (2.105)$$

$$F^{\uparrow}_{clr}(p) = B(T(p)) + G(p,p_s,T_s) - G(p,p_s,T(p_s)) + \int_{T(p)}^{T(p_s)} \frac{\partial G(p,p',T(p'))}{\partial T} dT(p') \qquad (2.106)$$

where

$$B(T(p)) = \int_{\Delta\nu} B_\nu(T)\, d\nu \qquad (2.107)$$

$$G(p,p',T) = \int_{\Delta\nu} \tau_\nu(p,p')\, B_\nu(T)\, d\nu \qquad (2.108)$$

$$\frac{\partial G(p,p',T)}{\partial T} = \int_{\Delta\nu} \tau_\nu(p,p') \frac{\partial B_\nu(T)}{\partial T}\, d\nu \qquad (2.109)$$

$T(p_s)$ = air temperature at surface pressure p_s

If the spectral width $\Delta\nu$ of the band is sufficiently narrow, $B_\nu(T)$ may be replaced by a mean value of the Planck function. The equation for G becomes

$$G(p,p',T) = \frac{B(T)}{\Delta\nu} \int_{\Delta\nu} \tau_\nu(p,p')\, d\nu \qquad (2.110)$$

In order to evaluate the G function for the fluxes, it is necessary to determine the

diffuse transmittance.

Chou and Peng (1983) and Chou (1984) defined the molecular line absorption and the e-type absorption (continuum absorption) for the computation of the diffuse-transmittance function due to water vapor and CO_2. The spectral ranges for both the molecular line absorption and the e-type absorption are classified as the band-centers (i.e., regions of strong absorption) and the band-wings (i.e., regions of moderate absorption). Following Chou and Peng (1983) and Chou (1984), broadband transmission functions for each of the absorbers is derived by averaging the diffuse-transmittance function associated with molecular line absorption and the diffuse-transmittance associated with e-type absorption over wide spectral intervals. The Planck-weighted broadband transmission functions are used for the water-vapor bands, while for the CO_2 bands, the broadband transmission functions are computed by integrating the diffuse-transmittance over the entire spectral interval. As a further simplification, Chou and Peng (1983) and Chou (1984) fitted the broadband transmission function for water vapor and CO_2 to analytical functions.

The broadband transmission functions for O_3 is based on the formulation given by Rodgers (1968). Rodgers fitted the integrated absorption of 9.6 μm O_3 band to an analytical form with the Lorentz line-shape transmission function for the random model. With these simplifications, the regression relations for the broadband transmission function for O_3 are obtained.

2.4.2.2 Water vapor bands

According to Chou and Peng (1983), the diffuse transmittance associated with molecular line absorption between pressure levels p and p′ at wavenumber ν is

$$\tau_\nu(p,p') = \tau_\nu(w) = 2\int_0^1 \exp[-k(p_r,T_r)\, w(p,p')/\mu]\, \mu\, d\mu \qquad (2.111)$$

where

k = molecular line absorption coefficient

μ = cosine of the zenith angle

p_r = reference pressure from Chou (1984)

T_r = reference temperature from Chou (1984)

w = scaled water vapor amount and is given by

$$w(p_1,p_2) = \frac{1}{g}\int_{p_1}^{p_2} \left(\frac{p}{p_r}\right) \exp[r(T - T_r)]\, q(p)\, dp \qquad (2.112)$$

where

r = factor from Chou (1980)

q = water vapor mixing ratio.

The diffuse transmittance associated with e-type absorption is

$$\tau_\nu(p,p') = \tau_\nu(u) = 2\int_0^1 \exp[-\sigma_\nu(T_0)\, u(p,p')/\mu]\, \mu\, d\mu \qquad (2.113)$$

where

σ = e-type absorption coefficient

u = scaled water vapor amount and is given by

$$u(p_1,p_2) = \frac{1}{g}\int_{p_1}^{p_2} e(p) \exp\left[1800\left(\frac{1}{T(p)} - \frac{1}{T_0}\right)\right] q(p)\, dp \qquad (2.114)$$

where

$e(p)$ = water vapor pressure in atmospheres

Therefore, the "Planck weighted" transmission function is

$$\tau(w,u;T) = \frac{1}{B(T)} \int B_\nu(T)\, \tau_\nu(w)\, \tau_\nu(u)\, d\nu \qquad (2.115)$$

Since $\tau_\nu(w,u;T)$ is a slowly varying function of temperature, it can be fitted by the quadratic function (Chou, 1984). The regression equation for broad transmission function for the band-wings is then:

$$\tau_\nu(w,u;T) = \tau(w,u;250)\,[1 + \alpha(w,u)\,(T - 250) + \beta(w,u)\,(T - 250)^2] \qquad (2.116)$$

where

$\alpha(w,u)$ = regression coefficient, given by Chou (1984)

$\beta(w,u)$ = regression coefficient, given by Chou (1984)

$\tau(w,u,250)$ = standardized transmission function, given by Chou (1984)

The regression equation for $\tau_\nu(w;T)$ for the band-centers is the same as for the band-wings but for $\tau(w;250)$, $\alpha(w)$ and $\beta(w)$.

The G function for the water-vapor band can be evaluated as

$$G_{WV_b} = B_{WV_w}(T)\, \tau(w;T) + B_{WV_c}(T)\, \tau(w,u;T) \qquad (2.117)$$

where

B_{WV_w} = spectrally integrated Planck blackbody functions over the band-wings

B_{WV_c} = spectrally integrated Planck blackbody functions over the band-centers

As mentioned earlier, the band-center absorption due to water vapor can be neglected

because it is dominated by molecular line absorption and the effect of e-type absorption is small.

For the 15 μm region, Chou (1984) fitted the diffuse transmission function integrated over the entire band. The diffuse transmission functions for water vapor molecular line and e-type absorption are, respectively,

$$\tau(w) = \exp\left[-6.7w/(1 + 16w^{0.6})\right] \tag{2.118}$$

$$\tau(u) = \exp\left[-27u^{0.83}\right] \tag{2.119}$$

The G function is given by

$$G_{WV15} = B_{15\mu m}(T)\ \tau(w)\ \tau(u) \tag{2.120}$$

For the 9.6 μm region, the molecular line absorption is weak and thus only the e-type absorption is considered. Chou (1984) also fitted the diffuse transmission associated with the e-type absorption in this region as

$$\tau(u) = \exp\left[-9.79u\right] \tag{2.121}$$

The G function is given by

$$G_{WV9.6} = B_{9.6\mu m}(T)\ \tau(w)\ \tau(u) \tag{2.122}$$

The G functions for water vapor in both the spectral regions represent part of the total

G function required to calculate the upward and downward longwave radiation fluxes.

2.4.2.3 CO_2 bands

The diffuse transmittance for CO_2 is obtained by using equation (2.111). That is

$$\tau_\nu(p,p') = \tau_\nu(w_c) = 2\int_0^1 \exp\left[-k_\nu(p_r,T_r)\, w_c(p,p')/\mu\right] \mu \, d\mu \qquad (2.123)$$

where

$w_c(p,p')$ = scaled CO_2 amount and is given by

$$w_c(p_1,p_2) = \frac{1}{g}\int_{p_1}^{p_2} c(p)\, f(p,T(p))\, dp \qquad (2.124)$$

where

$c(p)$ = CO_2 concentration

Equation (2.123) treats an inhomogeneous atmosphere as a homogeneous atmosphere with a constant pressure and temperature of p_r and T_r . This is possible because equation (2.124) scales the CO_2 concentration to simulate the absorption in an inhomogeneous atmosphere.

Chou and Peng (1983) fitted the spectrally averaged diffuse transmittance to analytical function. Their fitting function was

$$\tau(w_c) = \exp\left[-aw_c/(1 + bw_c^n)\right] \qquad (2.125)$$

where a, b, and n are constants chosen for individual spectral intervals. Parameter a is taken to be 3.1 for the band-centers, 0.08 for the narrow band-wings, and 0.04 for the

wide band-wings. The constant b is taken to be 15.1 for the band-centers, and 0.9 for the band-wings. Lastly, the parameter n is taken to be 0.56 for the band-centers, 0.55 for the narrow band-wings, and 0.57 for the wide band-wings.

In order to account for radiative cooling due to CO_2 in the stratosphere, Chou and Peng (1983) used the scaling function given by

$$f(P,T) = \left[\frac{p}{p_r} \right]^m R(T, T_r) \tag{2.126}$$

where,

m = parameter for correcting the error arising from the assumption of linear dependence of the absorption coefficient on pressure.

$R(T,T_r)$ = temperature scaling factor and is given by

$$R(T,T_r) = \exp [r(T - T_r)] \tag{2.127}$$

where

r = 0.0089 for the band-centers and 0.025 for the band-wings

T_r = 240 K for both the band-centers and the band-wings

Since the pressure scaling in equation (2.126) assumes that the absorption coefficient follows the Lorentz line-shape transmission function (equation (2.129)), this assumption is not valid at low pressures where broadening of absorption lines due to Doppler shift is important. In the 15 μm spectral region the height where line broadening due to molecular collision and Doppler shift are equally important is approximately 10 mb. For a Doppler line function the absorption is independent of pressure. To account for the Doppler effect, we define a critical pressure level, p_c. At pressures higher than this critical pressure, the absorption coefficient is independent of

pressure. We may now rewrite equation (2.126) as

$$f(p,T) = \left[\frac{p_c}{p_r} \right]^{m} R(T,T_r) \quad , \text{ for } p > p_c \tag{2.128}$$

where m is 0.85 for the band-centers and the narrow band-wings, 0.50 for the wide band-wings, and p_c is 1 mb for both the band-centers and band-wings (Chou and Peng, 1983).

2.4.2.4 Ozone bands

Rodgers (1968) defines a transmission function for a Lorentz line shape as

$$\tau(w_o) = \exp\left[- \frac{\pi\alpha p}{2\delta} \left\{ \left[1 + \frac{4k_i w_o}{\pi\alpha p} \right]^{\frac{1}{2}} - 1 \right\} \right] \tag{2.129}$$

where

α = line width at one atmosphere in cm^{-1}

δ = mean spectral interval in cm^{-1}

k_i = line strength in cm/g

w_o = ozone concentration in g/cm^2

With further simplification, Harshvardhan and Corsetti (1984) fitted the transmission function to an analytical function as

$$\tau(w_0) = 1 - 0.677 \left[1 - \exp \left\{ -4.398\tilde{p}\left(1 + 79.4 \left(\frac{w_0}{\tilde{p}}\right)^{\frac{1}{2}}\right) - 1 \right\} \right] \tag{2.130}$$

where

$$w_0 = \frac{1}{g}\int_{p_1}^{p_2} O_3 \, dp \tag{2.131}$$

$\tilde{p}$ = effective broadening pressure is given by

$$\tilde{p} = \frac{1}{1013.25} \frac{\int_{p_1}^{p_2} O_3 \; pdp}{\int_{p_1}^{p_2} O_3 \; dp} \tag{2.132}$$

where O_3 is the ozone mixing ratio.

In summary, broadband transmission functions in this model are separately calculated for three bands: water vapor, 15-μm, and 9.6-μm bands. Water vapor band is partitioned into two bands. One partition is for the band-centers in which the molecular absorption is much stronger than e-type absorption, so that e-type absorption can be neglected for the band-centers. The other is for the band-wings where both types of absorptions are included. In the 15-μm band, CO_2 absorption, water vapor molecular absorption, and water vapor e-type absorption are present. In the 9.6-μm band, water vapor molecular absorption is neglected. Thus the total absorption is due to ozone and water vapor e-type absorption. Given the broadband transmission functions, the spectrally integrated Planck blackbody function over each band can be obtained. Finally, the spectrally integrated Planck blackbody function for the upward and downward long-wave radiation fluxes is obtained by adding functions for each band. Formally, this is given by

$$B(T(p)) = B_{WV_c}(T(p)) + B_{WV_w}(T(p)) + B_{15\mu m}(T(p)) + B_{9.6\mu m}(T(p)) \tag{2.133}$$

Similarly, the total G function is given as a sum of G function for each band. That is

$$G(p,p',T) = G_{WV_w} + G_{15\mu m} + G_{9.6\mu m} \tag{2.134}$$

A similar expression for $\partial G/\partial T$ can also be obtained.

To account for the effect of cloudy skies, the probability for a clear line of sight is defined. The equations for cloudy skies are given by

$$F^{\downarrow}_{cld}(p) = B(T(p)) - C(p,p_s)\, G(p,p_t,T(p_t)) + \int_{T(p)}^{T(p_t)} C(p,p') \frac{\partial G(p,p',T(p'))}{\partial T} dT(p') \tag{2.135}$$

$$F^{\uparrow}_{cld}(p) = B(T(p)) - C(p,p_s)\, [G(p,p_s,T_s) - G(p,p_s,T(p_s))] + \int_{T(p)}^{T(p_s)} C(p,p') \frac{\partial G(p,p',T(p'))}{\partial T} dT(p') \tag{2.136}$$

where $C(p,p')$ is the probability for clear line of sight from p to p′.

This probability depends on the kind of cloud overlap present between two pressure levels. In this model a random overlap is used to compute the probability for clear line of sight. It is equal to the product of all fractional cloud amounts for all levels that have clouds (i.e., $N(3) \times N(4) \times \ldots$). It should be noted that the minimum clear line of sight for a random overlap atmosphere is $(1 - N(3)) \times (1 - N(4)) \times \ldots$

2.5 Modification to cumulus convection

An examination of model forecasted cloud amount and type showed dissipation of clouds with the time (Krishnamurti *et al.*, 1988). The reason for this was found to

be the drying of atmosphere in the upper layers. A careful analysis of model output showed that the drying was occurring primarily in regions of tropical convection.

The FSUGSM has a modified Kuo cumulus parameterization scheme for deep convection (detailed in section 2.2.2). The drying in the upper layers of the model atmosphere was due to excessive removal of the moisture needed for precipitation and moistening processes by the convective scheme. The scheme was modified to remove more moisture from lower levels with higher specific humidity than from the upper levels. It was found that by scaling the moistening term in each layer by a function proportional to $q^{3/2}$, the undesirable dissipation of clouds was removed. Thus the change in specific humidity at any level due to convective process is given by

$$(\Delta q)_k = a_q \frac{(q_c(k) - q(k))}{\Delta \tau} - bI_L \frac{q^{3/2}(k)}{\bar{q}_c} \tag{2.137}$$

where k represents a model level, and $\bar{q}_c$ is a column integral of specific humidity given by

$$\bar{q}_c = \frac{1}{g} \int_{p_t}^{p_b} q^{3/2} \, dp \tag{2.138}$$

The remaining symbols are explained in section 2.2.2. Therefore, the total moisture change removed, Q_{qr}, is given by

$$Q_{qr} = \frac{1}{g} \int_{p_t}^{p_b} \Delta Q_q \, dp \tag{2.139}$$

or

$$= \frac{1}{g}\int_{p_t}^{p_b} \left\{ a_q \frac{(q_s - q)}{\Delta\tau} - bI_L \frac{q^{3/2}}{\bar{q}_c} \right\} dp \qquad (2.140)$$

This formulation results in the moisture needed for moistening being removed from the layers with higher water content.

The above modification to the cumulus convection parameterization was tested using the T42 FSUGSM. The modified scheme achieves the desired end in that the resulting globally averaged total cloud amount remains steady. This is in accord with what would be expected in the real atmosphere.

CHAPTER III

PHYSICAL INITIALIZATION

3.1 Introduction

Although the current data coverage in the operational World Weather Watch (WWW) includes surface based networks of radiosonde, rawinsonde and pilot balloon distributions, diverse asynoptic surface and space based system such as commercial ships and aircrafts observations, soundings from the polar orbiting satellites, and cloud-tracked winds from the geostationary satellites, there still exist large data gaps over both continental and oceanic areas of the tropics as shown in Krishnamurti *et al.* (1991). The initial conditions used in NWP over these areas are largely derived from the first guess provided by a short forecast from a previous cycle of the data assimilation system. However, due to model imperfections the quality of the analyses over data gap regions are, therefore, likely to be lower than over data rich regions.

The sparsity of data results in large errors in the divergent wind which compounds humidity errors through moisture convergence. During the initial hours of model integration the divergent motion, diabatic heating, and surface pressure fields undergo an adjustment in response to the low equilibration of the humidity field. This is the period of so-called model spin-up. Such initial deficiencies in the humidity analysis are not addressed by the 'dynamical' type of initialization procedures. In this context there is a need for enhancement of the information content of the initial

moisture field. Physical initialization is a scheme that has been developed to do this.

3.2 Description of physical initialization

The term "physical initialization" was first introduced by Krishnamurti *et al.* (1984). The details of the initialization procedure are presented in Krishnamurti *et al.* (1991). The initialization procedure includes the following computations:

1) diagnostic measures of the surface fluxes of sensible heat and moisture according to Yanai *et al.* (1973),
2) generation of data sets of the potential temperature and the moisture variable on top of the constant flux layer consistent with the prescribed fluxes by using the reverse similarity theory,
3) an analysis of the humidity variable above the constant flux layer consistent with the imposed precipitation rates by the reverse cumulus parameterization, and
4) a matching of the earth's radiation budget as inferred from the radiation algorithm and as measured by the satellites. This procedure is completed by a Newtonian relaxation of all the basic variables of the model following a procedure outlined in Krishnamurti *et al.* (1988). This procedure is schematically illustrated in Figure 3.1. In the proceeding sections the initialization scheme following Krishnamurti *et al.* (1991) is described in detail.

3.2.1 Yanai fluxes

The surface fluxes of sensible heat (F_S) and moisture (F_L) following Yanai *et al.* (1973) may be expressed by relations,

$$F_S^{\uparrow} = \hat{Q}_1 - \hat{Q}_R - LP \tag{3.1}$$

$$F_L^{\uparrow} = LP - \hat{Q}_2 \tag{3.2}$$

where $\hat{Q}_1$, $\hat{Q}_R$ and $\hat{Q}_2$ denote the vertically integrated apparent heat source, net radiative heating, and apparent moisture sink, respectively, and P the observed rainfall rate.

The apparent heat source and the apparent moisture sink are defined as

$$Q_1 = \frac{\partial \overline{s}}{\partial t} + \nabla \cdot \overline{sv} + \frac{\partial}{\partial p} \overline{s\omega} \tag{3.3}$$

$$Q_2 = -L\left(\frac{\partial \overline{q}}{\partial t} + \nabla \cdot \overline{qv} + \frac{\partial}{\partial p} \overline{q\omega}\right) \tag{3.4}$$

where $\bar{s}$ is the large scale dry static energy.

3.2.2 Reverse similarity theory

The similarity theory calculates the surface fluxes of heat and moisture by using the similarity exchange coefficients with the known model variables (momentum, heat and moisture) on the top and bottom of the surface layer. The reverse similarity theory calculates the temperature and moisture variable on the top of surface layer by using the same similarity exchange coefficients with the prescribed surface fluxes of heat and moisture.

Given the Yanai fluxes of sensible and latent heat as an input to the similarity theory, we can solve for the potential temperature and the moisture variable on top of the constant flux layer. Different sets of similarity equations describe the stable and the unstable layers.

Following Chang (1978), the similarity fluxes of momentum, heat and moisture

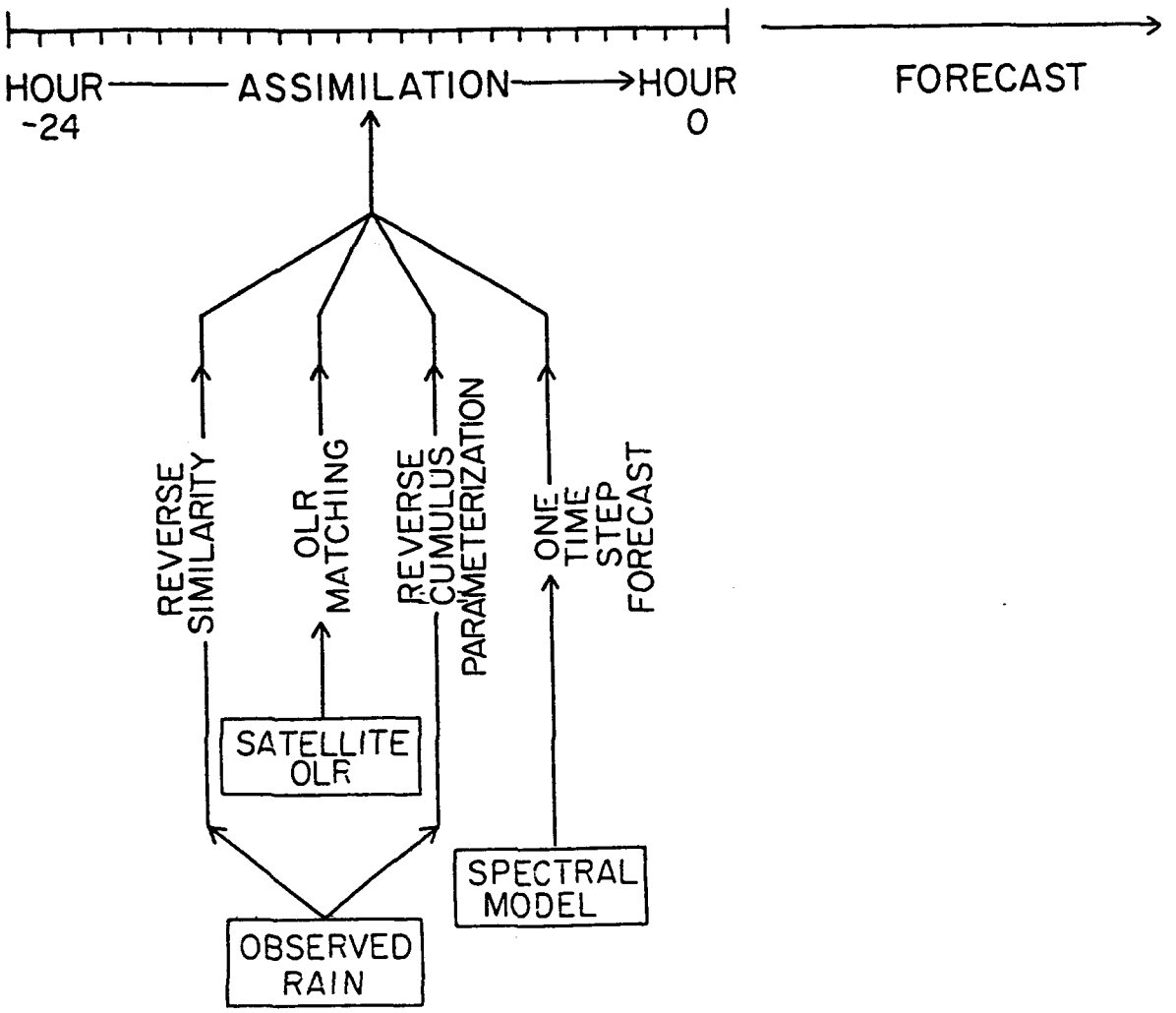

Figure 3.1 An outline of the physical initialization within the assimilation phase of the global model. The package of reverse similarity, OLR matching, reverse cumulus parameterization slides from left (hour-24) to right (hour 0) during this initialization period (from Krishnamurti *et al.*, 1994).

are given by the relations

$$F_M = \rho C_M (U_2 - U_1)^2 \tag{3.5}$$

$$F_H = \rho C_p C_H (U_2 - U_1)(\theta_2 - \theta_1) \tag{3.6}$$

$$F_Q = \rho C_q (U_2 - U_1)(q_2 - q_1) g_w \tag{3.7}$$

where the similarity exchange coefficients are expressed as follows:

For the stable and neutral case: $R_{i_B} > 0$

$$C_M = \frac{U_*^2}{(U_2 - U_1)^2} = \frac{k^2}{[\ln(Z_2/Z_1)]^2 (1 + 4.7 R_{i_B})^2} \tag{3.8}$$

$$C_H = \frac{U_* \theta_*}{(U_2 - U)(\theta_2 - \theta_1)} = \frac{-k^2}{0.74[\ln(Z_2/Z_1)]^2 (1+4.7 R_{i_B})^2} \tag{3.9}$$

$$C_q = 1.7\, C_H \tag{3.10}$$

For the unstable case: $R_{i_B} < 0$

$$C_M = \frac{U_*^2}{(U_2 - U_1)^2} = \frac{k^2}{[\ln(Z_2/Z_1)]^2} \left(1 - \frac{9.4 R_{i_B}}{1+C|R_{i_B}|^{\frac{1}{2}}}\right) \tag{3.11}$$

$$C_H = \frac{U_* \theta_*}{(U_2 - U_1)(\theta_2 - \theta_1)} = \frac{-k^2}{0.74[\ln(Z_2/Z_1)]^2} \left(1 - \frac{9.4R_{i_B}}{1+C|R_{i_B}|^{\frac{1}{2}}}\right) \qquad (3.12)$$

$$C_q = 1.7\, C_H \qquad (3.13)$$

where,

C_M, C_H, C_q = exchange coefficient of momentum, heat and moisture

U_* = friction velocity

θ_* = scaling temperature

Z_2, Z_1 = height of top and bottom of surface layer

U_2, U_1 = wind at top and bottom of surface layer

θ_2, θ_1 = potential temperature at top and bottom of surface layer

q_2, q_1 = moisture at top and bottom of surface layer

g_w = ground wetness

k = von Karman constant

R_{i_B} = bulk Richardson number which can be expressed as

$$R_{i_B} = \frac{g}{\bar{\theta}} \frac{(\theta_2 - \theta_1)(Z_2 - Z_1)}{(U_2 - U_1)^2} \qquad (3.14)$$

The expression for C follows the analysis of Louis (1979):

$$C = \frac{c_0 \times 9.4k^2}{[\ln(Z_2/Z_1)]^2} \left[\frac{Z_2}{Z_1}\right] \qquad (3.15)$$

where c_0 is taken to be 7.4 for momentum and 5.3 for heat and moisture.

To solve for θ_2 and q_2 given the surface fluxes of heat and moisture, the reverse

similarity theory is invoked with the assumption that the wind at the lowest model level U_2 is known. The only unknown in the equations (3.9) and (3.10) is θ_2.

For the stable case, equation (3.9) may be written as

$$4.7^2 R_{i_B}^2 + (9.4 - A)R_{i_B} + 1 = 0 \tag{3.16}$$

where

$$A = \frac{1}{0.74} \frac{\overline{\theta}}{g\Delta z} \frac{(U_2-U_1)^3}{U_* \theta_*} \frac{k^2}{[\ln(Z_2/Z_1)]^2} \tag{3.17}$$

The signs of both roots of the quadratic equation (3.16) are positive and the root with the larger value is beyond the physical upper limit of R_{i_B}. With R_{i_B} computed, θ_2 is then obtained from equation (3.14).

For the unstable case ($U_* \theta_* < 0$) the modified θ_2 is obtained by minimizing an objective function using the Newton-Raphson method. The objective function is defined by

$$F = \frac{U_* \theta_*}{(U_2-U_1)(\theta_2-\theta_1)} + C_H \tag{3.18}$$

Computation of new θ_2 is detailed in Krishnamurti *et al.* (1991). Once θ_2 is computed, C_H and C_q can then be obtained using equations (3.9), (3.10), (3.12) and (3.13), and q_2 is obtained from equation (3.7).

3.2.3 Reverse cumulus parameterization

The vertical distribution of specific humidity is reanalyzed such that the rainfall implied by the cumulus parameterization algorithm closely matches the prescribed

"observed" rainfall rates. The procedure for the construction of a reverse cumulus parameterization algorithm was discussed in Krishnamurti *et al.* (1988). This was designed for the modified Kuo scheme.

In the reverse Kuo (modified), the specific humidity q is modified as

$$q_m = \frac{R_0 \cdot q}{I_L} + \bar{q}\left[1 - \frac{R_0}{I_L}\right] \tag{3.19}$$

where q_m is the modified specific humidity, q is the specific humidity prior to modification, R_0 is the observed rainfall rate, $\bar{q}$ is the vertically averaged specific humidity expressed by

$$\bar{q} = \frac{-\frac{1}{g}\int_{p_b}^{p_t} q \, dp}{-\frac{1}{g}\int_{p_b}^{p_t} dp} \tag{3.20}$$

The remaining symbols are explained in Chapter II (section 2.2).

The convergence of the moisture which has been modified to q_m matches the observed rainfall R_0. Thus

$$-\frac{1}{g}\int_{p_b}^{p_t} \omega \frac{\partial q_m}{\partial p} dp = R_0 \tag{3.21}$$

The adjustment procedure is such that the total precipitable water in the column remains invariant. That is,

$$-\frac{1}{g}\int_{p_b}^{p_t} q_m \, dp = -\frac{1}{g}\int_{p_b}^{p_t} q \, dp \tag{3.22}$$

To obtain the analyzed rainfall, a mix of raingauge and OLR based regression methods is used. This method is described in the papers, Krishnamurti *et al.* (1983, 1991, 1993).

The reverse cumulus parameterization is only applied to the tropical latitudes between 30°S and 30°N.

3.2.4 Initialization of the earth's radiation budget

This initialization entails matching the OLR derived from radiation algorithm of the model with the satellite observed OLR. By introducing a structure function (with parameter ε) for the moisture variable above 500 mb, the local difference between two estimates of OLR can be minimized. This minimization determines an optimal value of ε. This procedure tends to improve the high and the middle clouds and the planetary albedo, thereby improving the overall radiation budget.

The minimization algorithm utilizes an iterative approach. For iteration ℓ we write

$$q^{\ell} = q^{\ell-1}(1 + \varepsilon^{\ell}) \tag{3.23}$$

where for $\ell = 0$, $q^0 = q$ (analysis).

The residue at the end of iteration ℓ-1 is defined by

$$R^{\ell} = OLR_{SAT} - OLR_M^{\ell} \tag{3.24}$$

where the subscript M denotes the model based value and SAT denotes the satellite based value.

The structure parameter at the ℓ^{th} iteration is computed by using the bisection method. This can be written by

$$\varepsilon^{\ell} = \frac{R^{\ell-1} \; F^{\ell-1}}{100} \tag{3.25}$$

where $F^{\ell-1}$ is the convergence factor at the iteration ℓ-1, which is given by

$$F^{\ell-1} = \frac{F^{\ell-2}}{2} \tag{3.26}$$

Here, an initial value of the convergence factor, F^0, is set to 1.

3.2.5 Newtonian relaxation

This initialization is carried out using a Newtonian relaxation (Hoke and Anthes, 1976) of the basic model variables during a preintegration phase.

The equation for the Newtonian relaxation takes the form,

$$\frac{\partial A}{\partial t} = F(A,t) + N(A,t)(A^0 - A) \tag{3.27}$$

where N denotes the relaxation coefficient, A^0 represents a future value of a variable A. F(A,t) is a forcing term of the equations for variable A.

The integrations are carried out in two steps. First, the tendencies for the normal forcing terms F are computed. The next step applies the Newtonian term. This is

expressed in finite difference form:

$$\frac{A(t+\Delta t) - A^{*}(t+\Delta t)}{2\Delta t} = N(A,t)\,[A^{0}(t+\Delta t) - A(t+\Delta t)] \qquad (3.28)$$

where $A^{*}(t+\Delta t)$ denotes a predicted value of A at time $(t+\Delta t)$ prior to the Newtonian relaxation. The Newtonian coefficients are time invariant during the integration. The values used in this study are those used in Krishnamurti *et al.* (1991): 1×10^{-4} sec^{-1} for both vorticity and surface pressure and 5×10^{-5} sec^{-1} for divergence. The relaxation coefficient for humidity field is taken to be 5×10^{-5} sec^{-1} for the surface layer. No relaxation of the humidity field is carried out above the surface layer.

3.3 Some previous results from physical initialization

A large number of studies examining the impact of physical initialization have been carried out. Most of these studies address the impact on rainfall analysis and forecast.

Krishnamurti *et al.* (1991) have illustrated the impact of physical initialization on medium range forecasts over the tropics. They showed that rainfall amounts and locations of heavy rainfall in 4-5 day forecasts from physically initialized initial fields exhibited close agreement with observed rainfall. Mathur *et al.* (1992) made an effort to study the impact of physical initialization with NMC model. They demonstrated a strong positive impact on tropical prediction from the inclusion of a reverse cumulus parameterization within the six hourly assimilation cycle. The improved initial state in the forecast model led to the enhancement of the forecast rain and circulation. Krishnamurti *et al.* (1993) have shown the improvement in nowcasting and short-range forecast skill of rainfall prediction by implementing the rainfall retrieval algorithm

using OLR, SSM/I, and raingauge measurements within the physical initialization. Krishnamurti et al. (1994) explored the impact of physical initialization on tropical rainfall assimilation and forecasts. They found that the mean nowcasting skill of rainfall exceeded the current operational skill.

CHAPTER IV

NUMERICAL EXPERIMENTS AND RESULTS

4.1 Initial data

In this study two different types of data have been used as an initial state for the cloud forecasts beginning at 12 UTC 20 October 1991. The first initial state is taken from ECMWF IIIb analyses. We refer to this as the normal or traditional initial conditions. The second initial state consists of data physically initialized by the FSUGSM.

4.1.1 The normal initial data

The ECMWF IIIb analyses provide the meteorological fields of height, zonal and meridional wind components, temperature, and relative humidity on 12 mandatory pressure levels (1000, 850, 700, 500, 400, 300, 250, 200, 150, 100, 70, and 50 mb). These analyses are produced by the 4-dimensional data assimilation system (an intermittent system) which uses a multivariate optimum interpolation analysis, a non-linear normal mode initialization and a high-resolution forecast that produces the first estimate for the subsequent analysis. The analysis is divided into two parts: one for the analysis of humidity and a second for the simultaneous analysis of geopotential, wind, and surface pressure. A complete description of the ECMWF data assimilation system is provided by Bengtsson *et al.* (1982).

4.1.2 Physically initialized data

Physical initialization was carried out during a pre-integration phase between day -1 (12 UTC 19 October, 1991) and day 0 (12 UTC 20 October, 1991) using the T106 FSUGSM. During the assimilation phase, ingestion of the observed rainrates and OLR matching are performed as shown in Figure 3.1. The observed rainrates are obtained from an algorithm (Krishnamurti *et al.*, 1993) that combines measurements of satellite-based OLR, SSM/I, and raingauge data.

A modification of the initial state variables via incorporation of analyzed tropical rainrates is accomplished during the assimilation phase of the model forecast. The physical initialization process produces, in a diagnostic sense, a thermodynamic consistency between the humidity variable, the surface fluxes, rainfall distributions, diabatic heating, and the clouds.

4.2 Results from global forecast experiments

Sensitivity of cloud predictive skill was tested in the FSUGSM as a function of both initial conditions and implicit versus explicit cloud schemes. Four experiments were designed as follows:

1) the experiment conducted with the implicit cloud scheme using the normal initial data ('control'),
2) the experiment with the same model as in 'control' but with the physically initialized data ('EXP1'),
3) the experiment conducted with the explicit cloud scheme using the normal initial data ('EXP2'), and
4) the experiment with the same model as in 'EXP2' but with the physically initialized data ('EXP3').

A six day forecast was made in each of these four experiments.

4.2.1 Initial clouds

4.2.1.1 Zonal mean of cloudiness

In Figure 4.1 the zonal-mean total cloudiness for two initial conditions is compared with the surface-based observations analyzed over land by Warren *et al.* (1986). The ground data were compiled from an eleven year data set extending 1971 to 1981. The observed values (Figure 4.1) show a maximum cloud cover near the equator and minimum in the subtropics of both hemispheres. This is a typical feature of ITCZ's seasonal position. Other peaks of maximum cloud cover were found near 60 and 60°N which are a result of middle latitude system such as cold fronts. The initial cloudiness based on the physical initialization shows better agreement in both the shape and location of the extreme values with the observed data than that of the normal initial data. In particular, in the tropics it shows a remarkable improvement in the amount compared with the normal initial data. Obviously it is the effect of physical initialization. Cloud amounts of the physically initialized data are consistently higher than those of the normal initial data in both hemispheres.

4.2.1.2 Geographical distribution of cloudiness

Figure 4.2 shows the initial high, middle, low and total cloud distributions with the normal data (left) and with the physically initialized data (right). A comparison of the distribution of cloudiness in the two initial conditions shows that the physically initialized data is more representative in terms of

1) the total cloud amount,

2) the deep convective cloud associated with the ITCZ and Southern Pacific

Convergence Zone (SPCZ) over active convective areas such as the western Pacific and northeast of Australia, and convective cloud over South America,

3) the high and low cloud amount in the middle latitudes (their location matches with the normal initial data),

4) the location and amount of high cloud both in the tropics and middle latitudes consistent with the improvement in convective cloud.

4.2.2 Comparison of control and EXP1

4.2.2.1 Global-mean cloudiness

Figure 4.3 shows the global-mean cloud cover for high, middle, low and total clouds as a function of forecast time for the control run and EXP1. Figure 4.3 (top) illustrates the fact that the cloud cover stabilizes slowly. This suggests a substantial spin-up time for model cloud cover. This is further illustrated by the following tabulation of the spin-up time for high, middle, low, and total clouds derived from Figure 4.3.

Table 4.1 Percent cloud cover and spin-up time for control and EXP1.

		Initial cloud cover (%)	Cloud cover after stabilization (%)	Spin-up time (days)
Control				
	High	11	25	3.5
	Middle	8	16	2.5
	Low	16	24	2.0
	Total	28	42	2.5
EXP1				
	High	24	24	0
	Middle	17	17	0
	Low	17	25	1.5
	Total	40	45	1.5

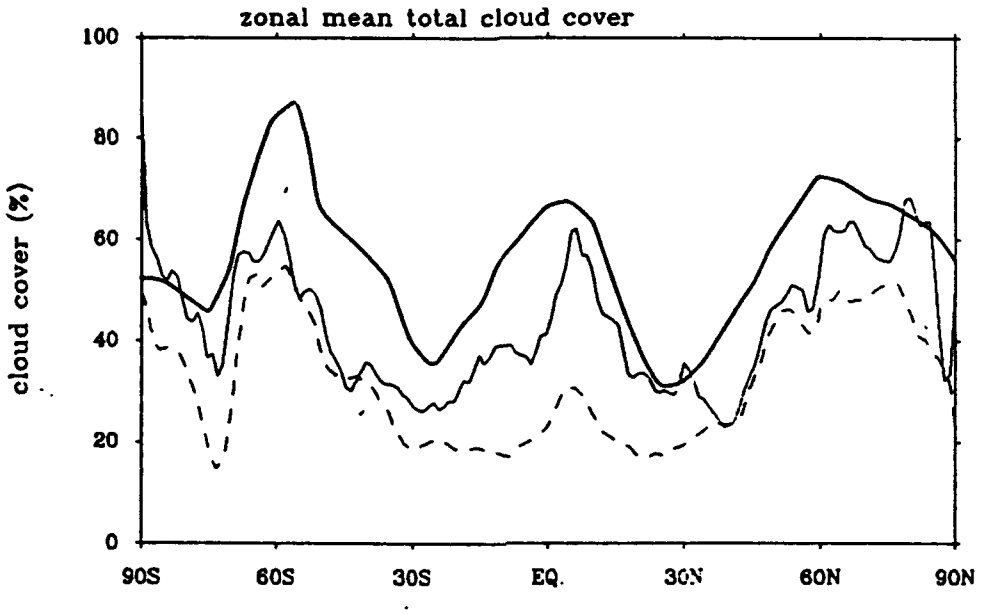

Figure 4.1 Comparison of the zonal-mean total cloudiness for the normal initial data (dashed line) and the physically initialized data (solid line) with a surface-based climatology (bold line).

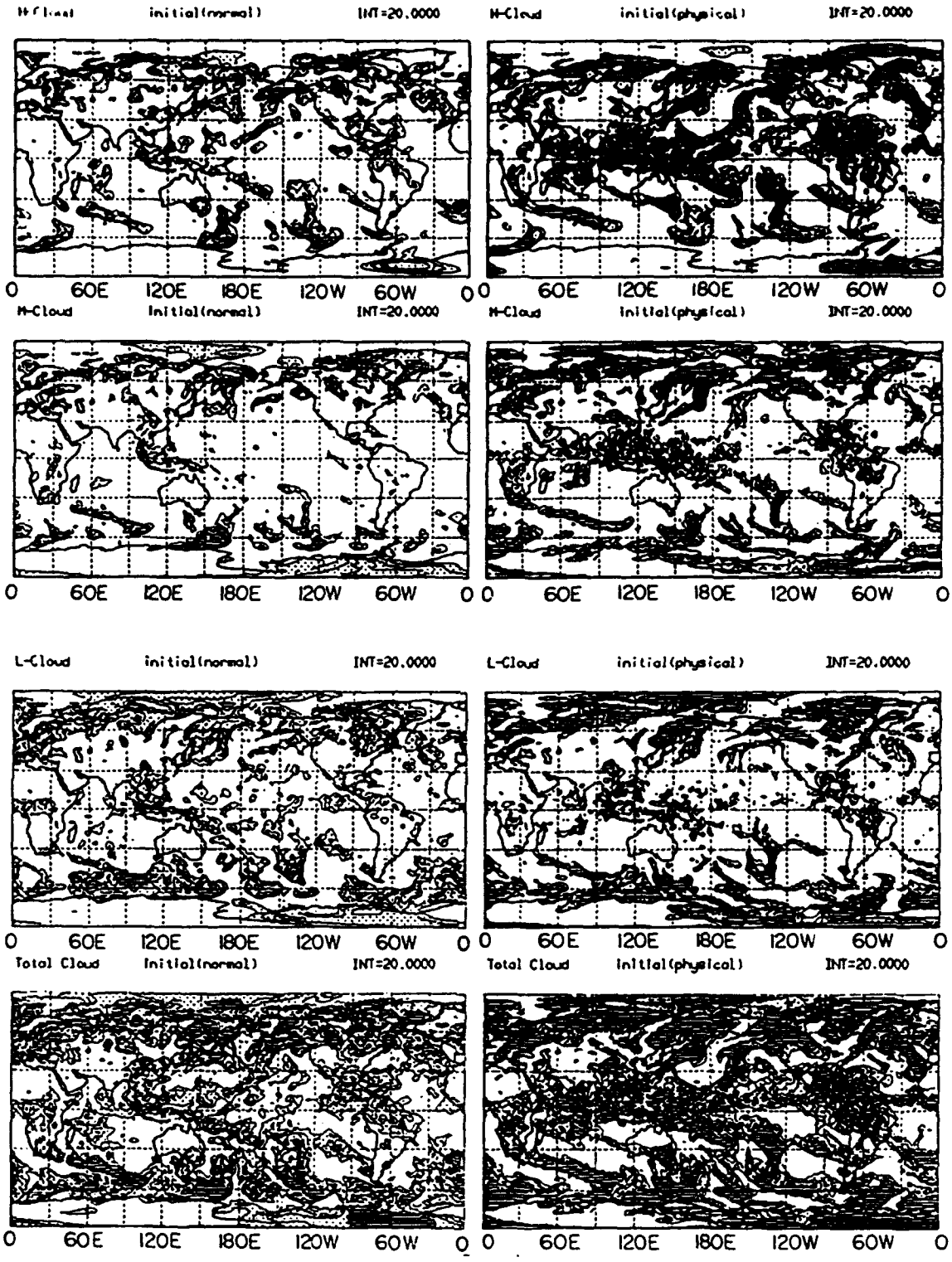

Figure 4.2 Global distribution of the initial high, middle, low and total clouds with the normal initial data (left) and with the physically initialized data (right). Contour interval is 20%. Values between 20% and 80% are dotted; values above 80% are shaded.

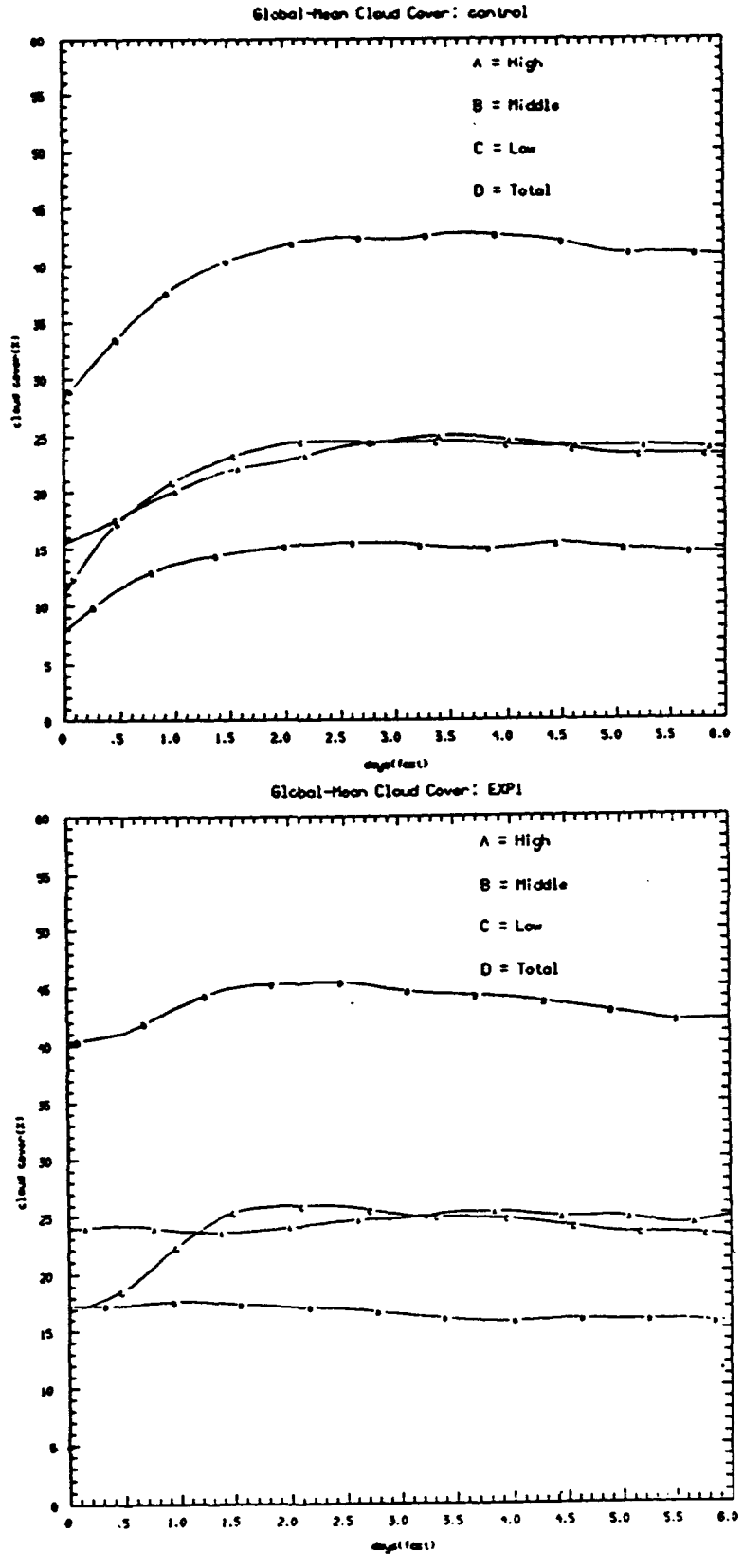

Figure 4.3 Global-mean cloud cover for high (A), middle (B), low (C) and total clouds (D) as a function of forecast time for the control run (top) and EXP1 (bottom),

Table 4.1 shows that the spin-up time for the high clouds is the highest followed by the middle clouds. Figure 4.3 (bottom) shows that in 'EXP1' high and middle clouds remain stable throughout the integration while the low clouds tend towards stabilization. The spin-up time in EXP1 is dramatically less than in control run. Also note that the total cloud cover in EXP1 (45%) is consistently higher than in the control run (42%). The former is closer to the observational estimate (about 50%) than the latter.

4.2.2.2 Geographical distribution of cloudiness

Figures 4.4(a) through 4.4(f) illustrate the global cloud cover distribution for the control run (left) and EXP1 (right). Discernible features such as the climatological cloud patterns associated with the ITCZ and SPCZ are the criteria for comparison between these experiments. It is seen from the figures that EXP1 shows a more robust SPCZ over north of Australia and Southeast Asia and ITCZ around 10°N over all 6 days of the forecast. Further, in EXP1 the minimal cloud cover over Middle East, North Africa and Central Asia is in consonance with climatological divergent circulations in the tropics (Krishnamurti *et al.*, 1983). Lastly, the bimodality in the cloud distribution over the tropical western and central Pacific (Ogura and Cho, 1973) is much more evident in EXP1 than the control.

4.2.3 Comparison of EXP2 and EXP3

4.2.3.1 Global-mean cloudiness

Figure 4.5 shows the global-mean cloud cover similar to Figure 4.3 for EXP2 and EXP3. As before, a tabulation of the spin-up time derived from Figure 4.5 is presented below.

Table 4.2 Percent cloud cover and spin-up time for EXP2 and EXP3.

		Initial cloud cover (%)	Cloud cover after stabilization (%)	Spin-up time (days)
EXP2				
	High	11	16	0.5
	Middle	8	12	2.0
	Low	16	30	3.0
	Total	28	39	2.5
EXP3				
	High	24	13	2.0 (decreased)
	Middle	17	14	1.0 (decreased)
	Low	17	30	2.5
	Total	40	41	2.5

The response of the explicit scheme to physically initialized data seems very irregular. There is an initial decay of the high and middle clouds, and an initial growth of low clouds before stabilization. This requires further investigation of the explicit scheme.

4.2.3.2 Geographical distribution of cloudiness

Figure 4.6 illustrates the high, middle, low and total cloud distributions predicted by the FSUGSM explicit scheme with normal initial data (left) and the physically initialized data (right).

Overall, high and middle clouds in both experiments, EXP2 and EXP3, tend to decrease over the tropics during the forecast. Deep convective clouds are not found over the tropics in EXP2, while in EXP3 only a few deep convective clouds are found in the western Pacific. An undesirable feature in both experiments is an increase in cloudiness, particularly low clouds, during the integration. Therefore, total cloud amounts are mostly composed of the low clouds.

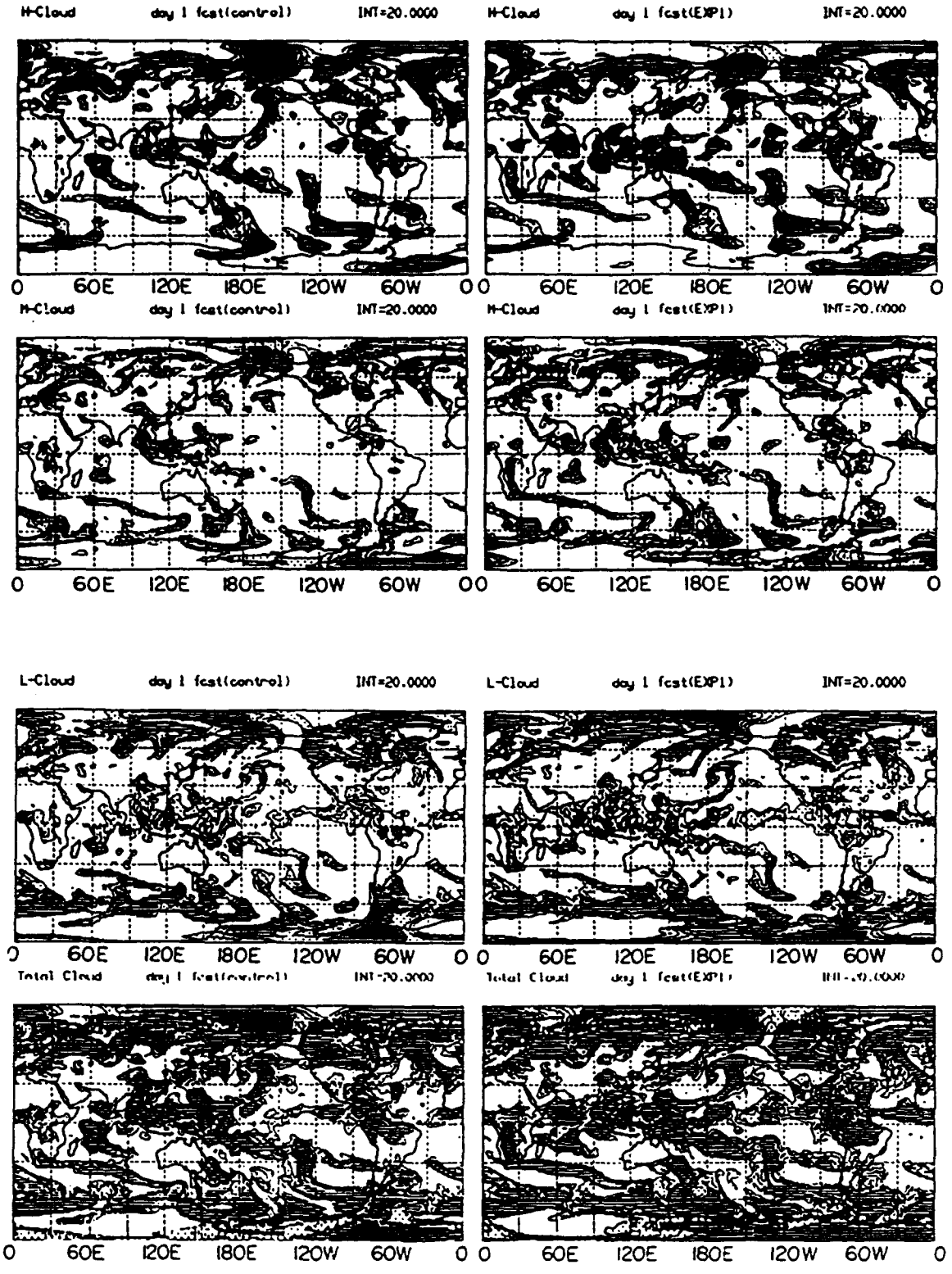

Figure 4.4(a) Global distribution of the high, middle, low and total clouds for day 1 forecast with the control run (left) and EXP1 (right). Contour interval is 20%. Values between 20% and 80% are dotted; values above 80% are shaded.

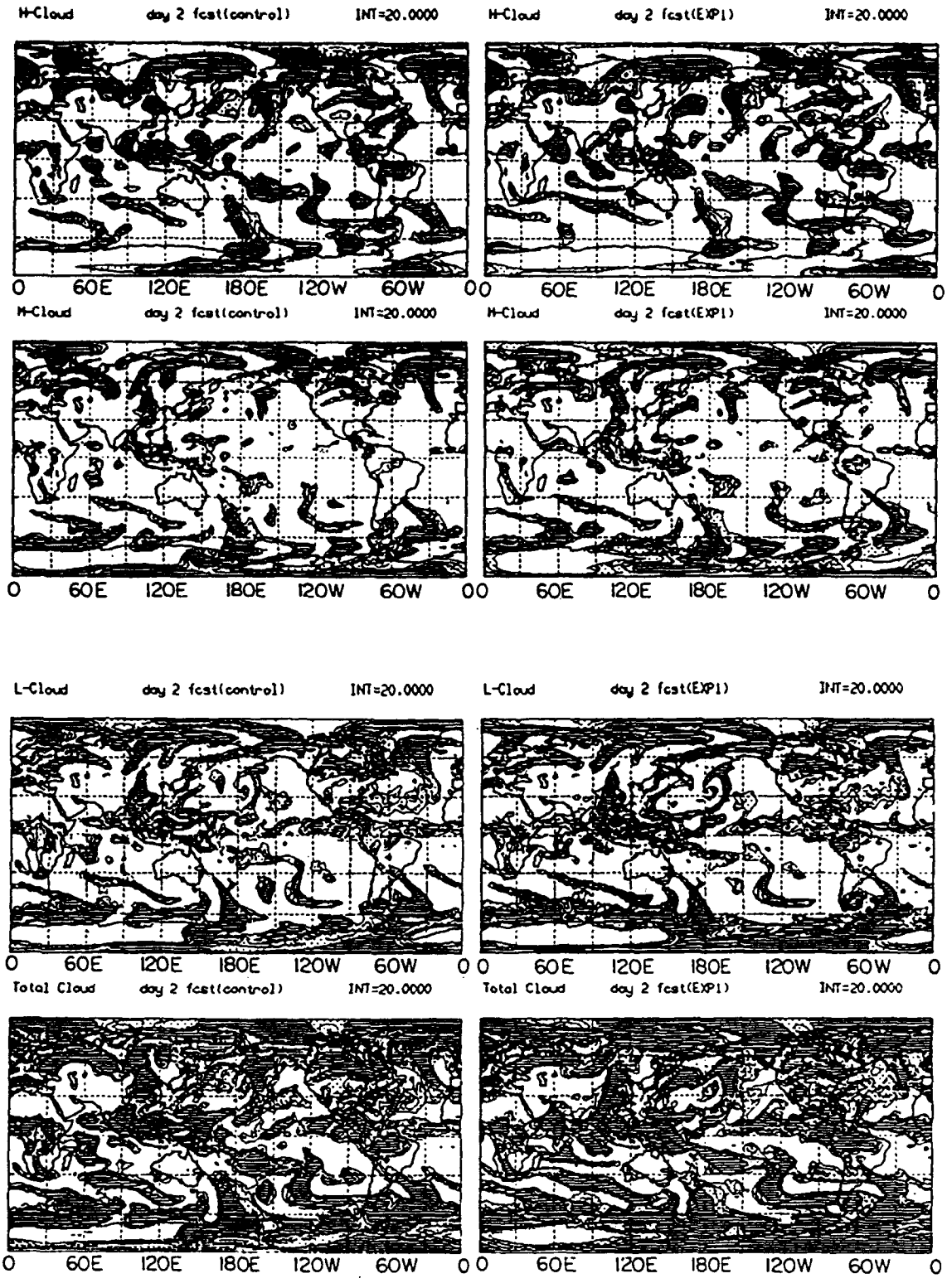

Figure 4.4(b) As Figure 4.4 (a) but for the day 2 forecast.

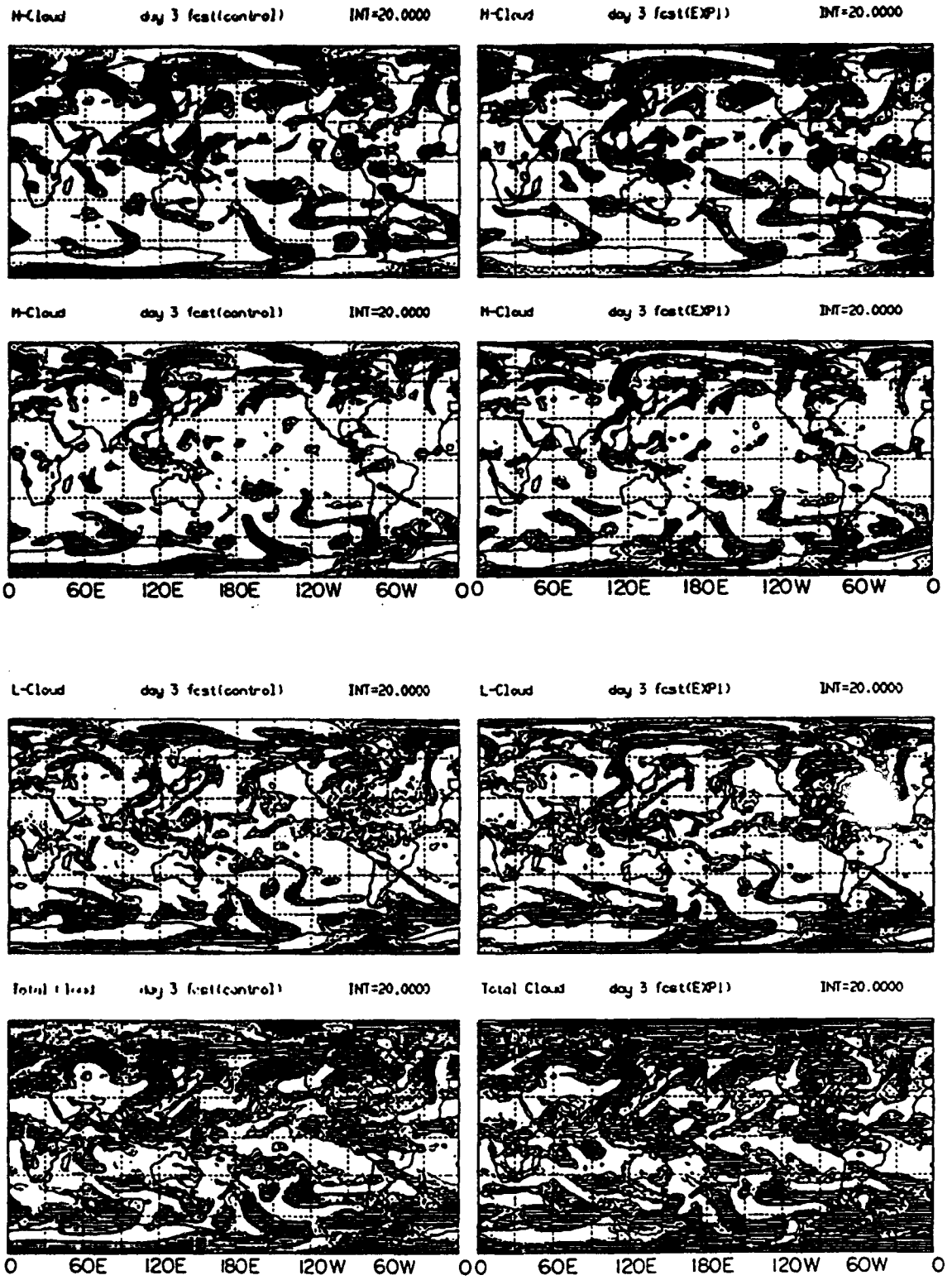

Figure 4.4(c) As Figure 4.4 (a) but for day 3 forecast.

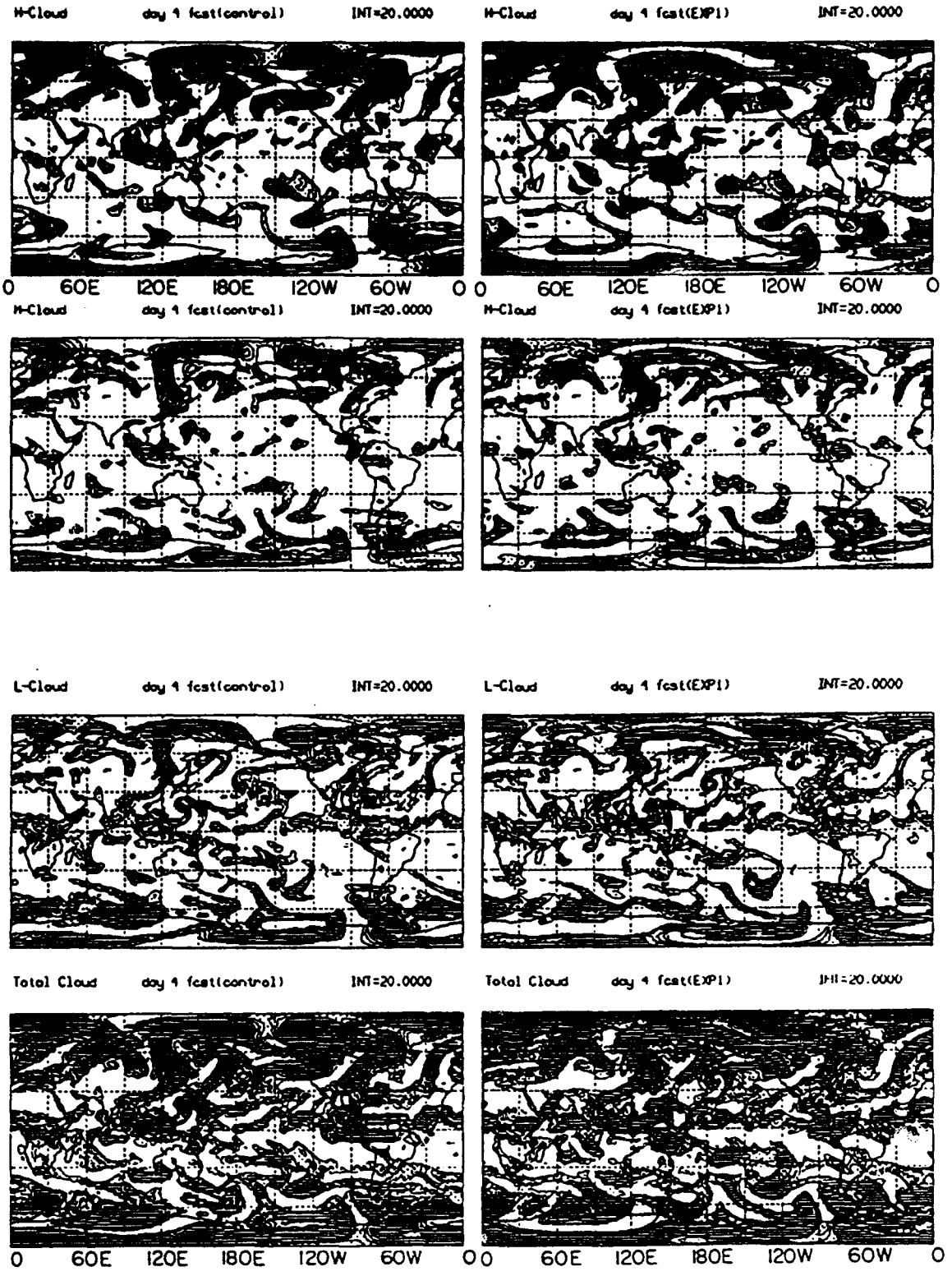

Figure 4.4(d) As Figure 4.4 (a) but for day 4 forecast.

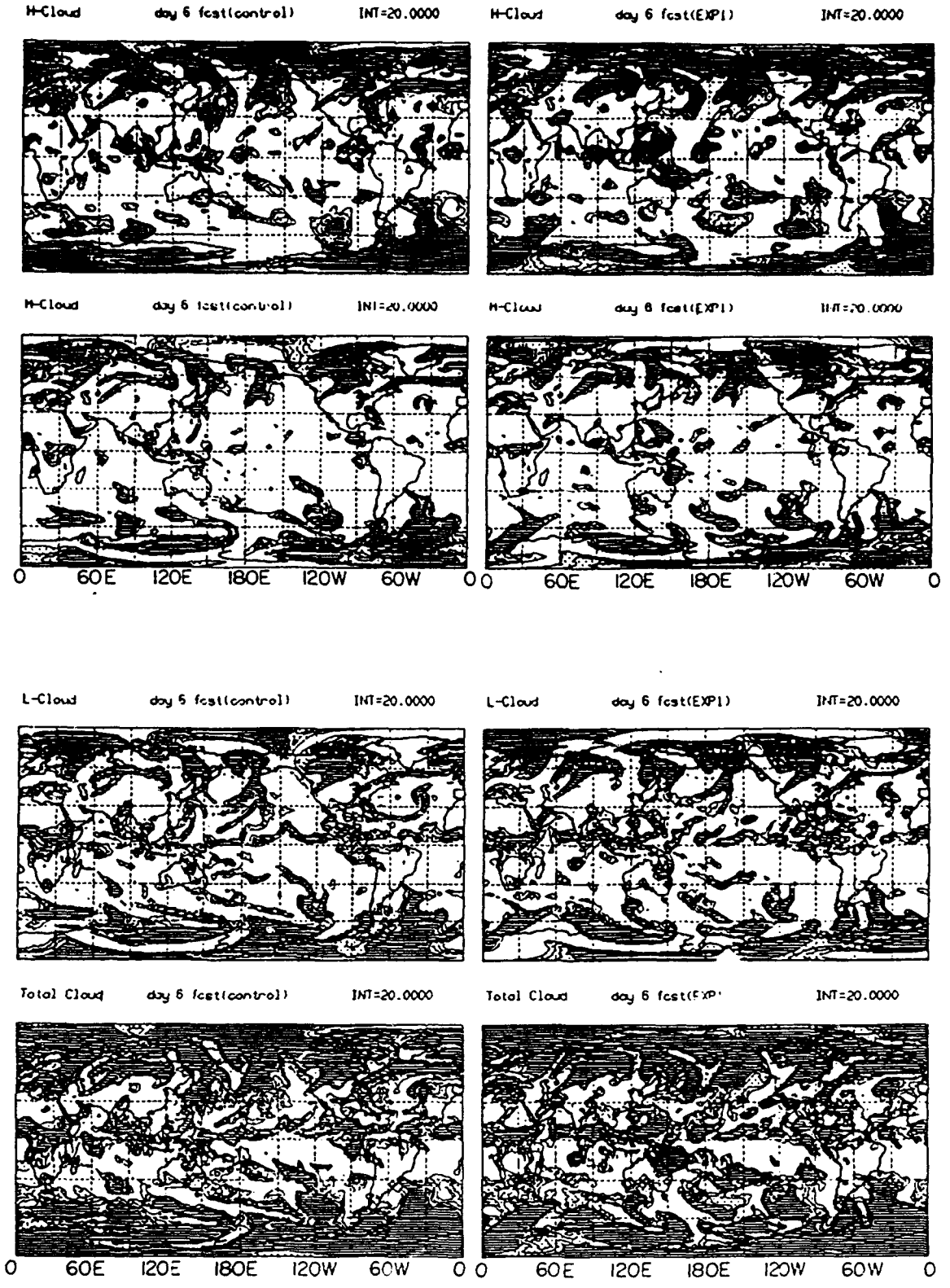

Figure 4.4(f) As Figure 4.4 (a) but for day 6 forecast.

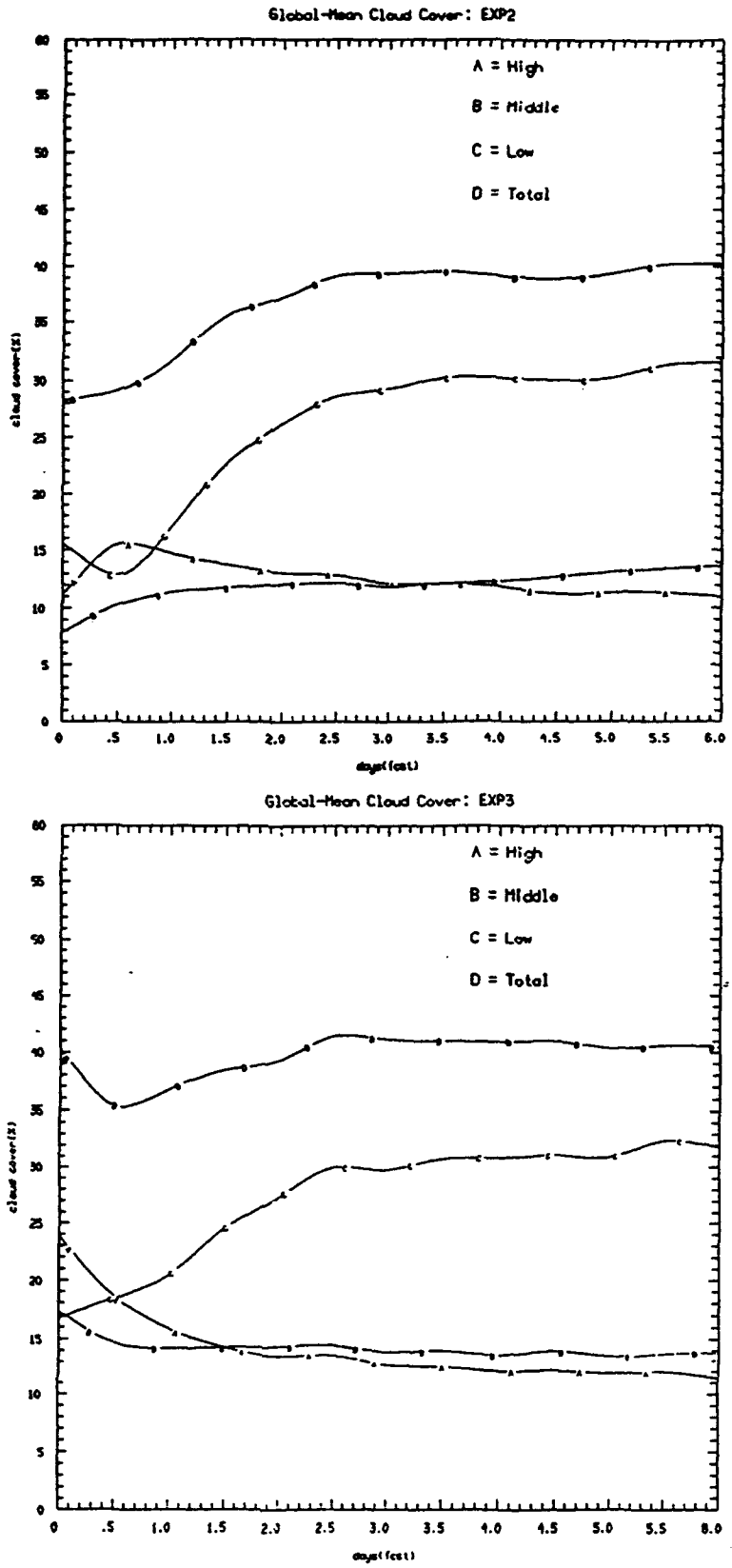

Figure 4.5 Global-mean cloud cover for high (A), middle (B), low (C) and total clouds (D) as a function of forecast time for EXP2(top) and EXP3(bottom).

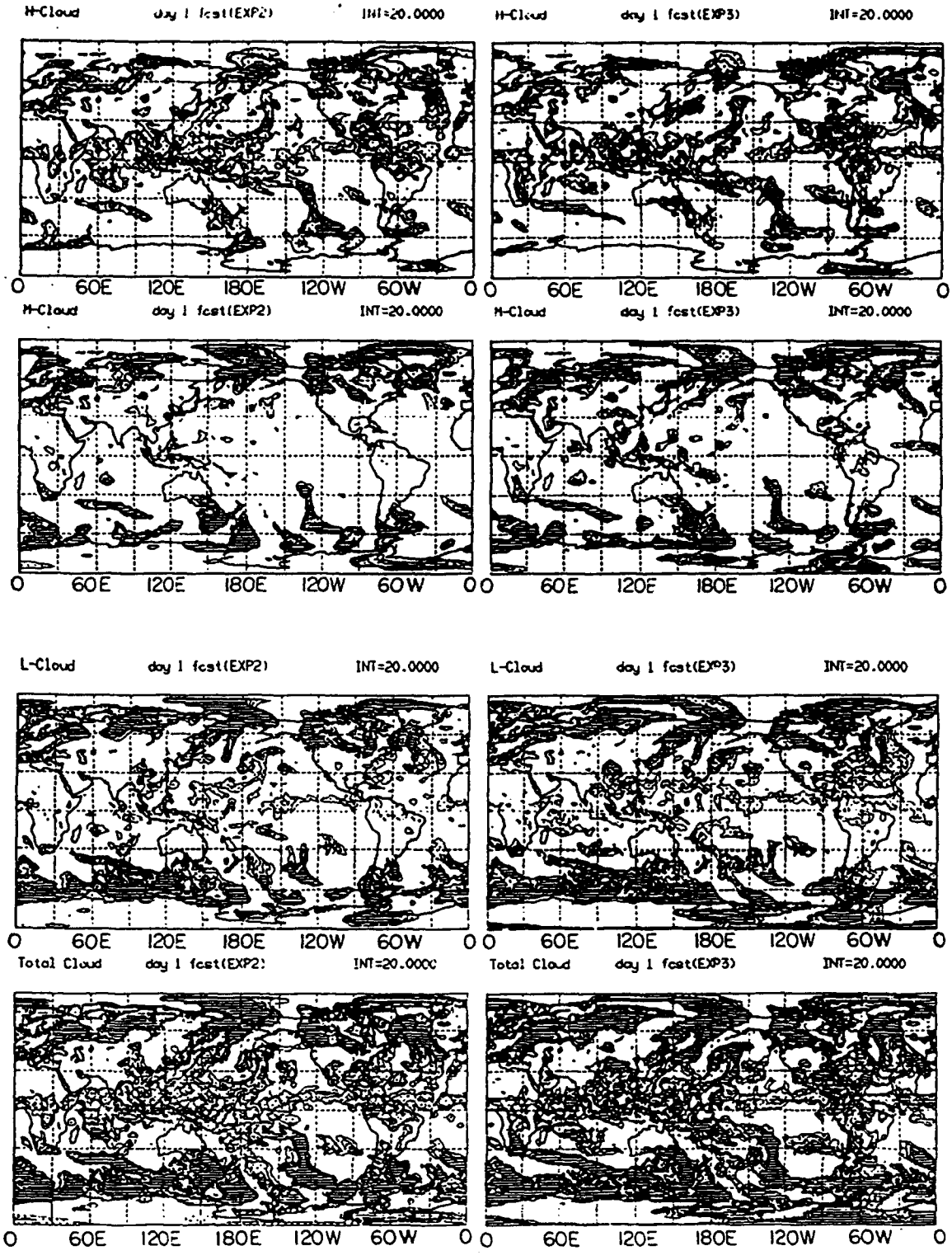

Figure 4.6(a) Global distribution of the high, middle, low and total clouds for day 1 forecast with the EXP2 (left) and EXP3 (right). Contour interval is 20%. Values between 20% and 80% are dotted; values above 80% are shaded.

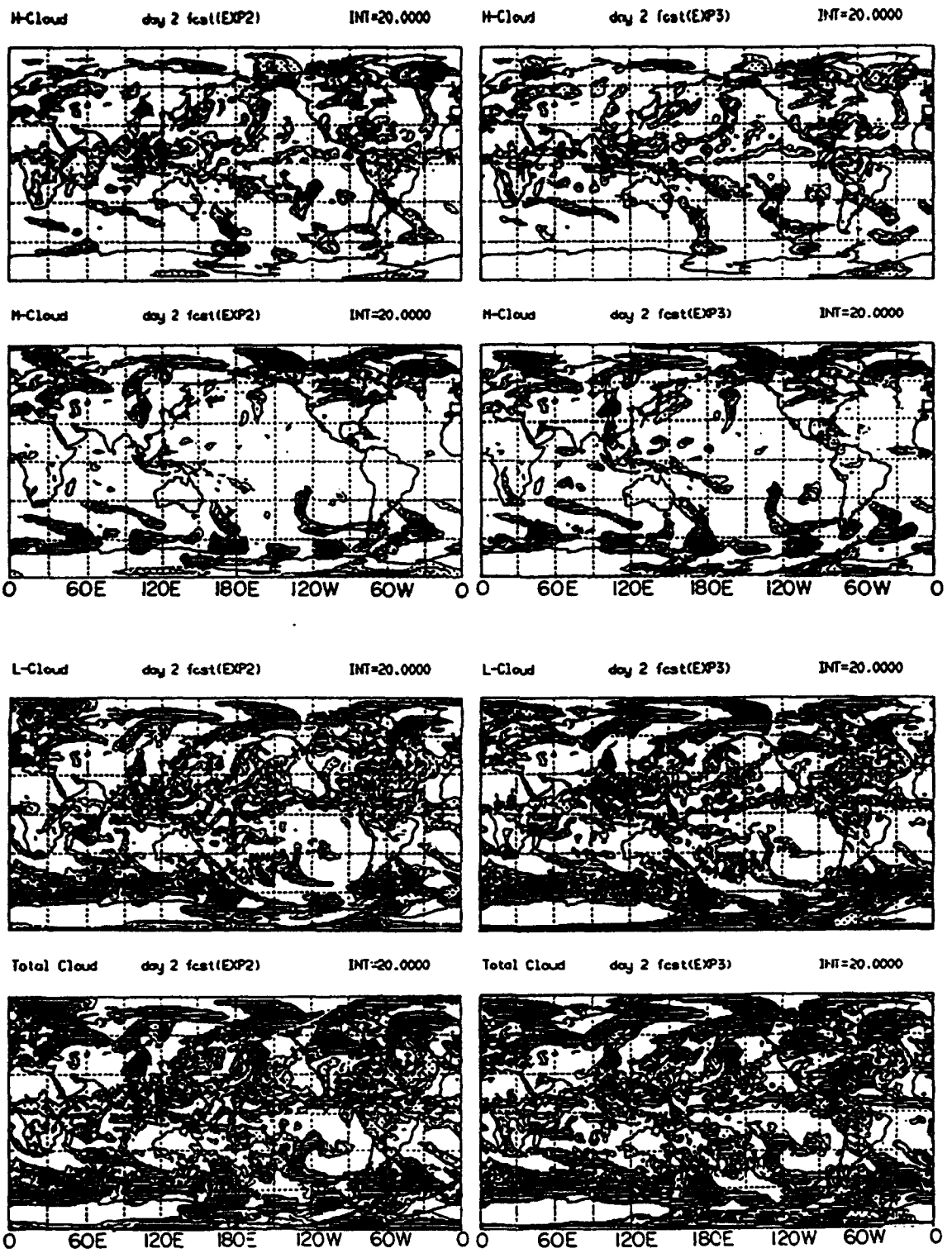

Figure 4.6(b) As Figure 4.6 (a) but for day 2 forecast.

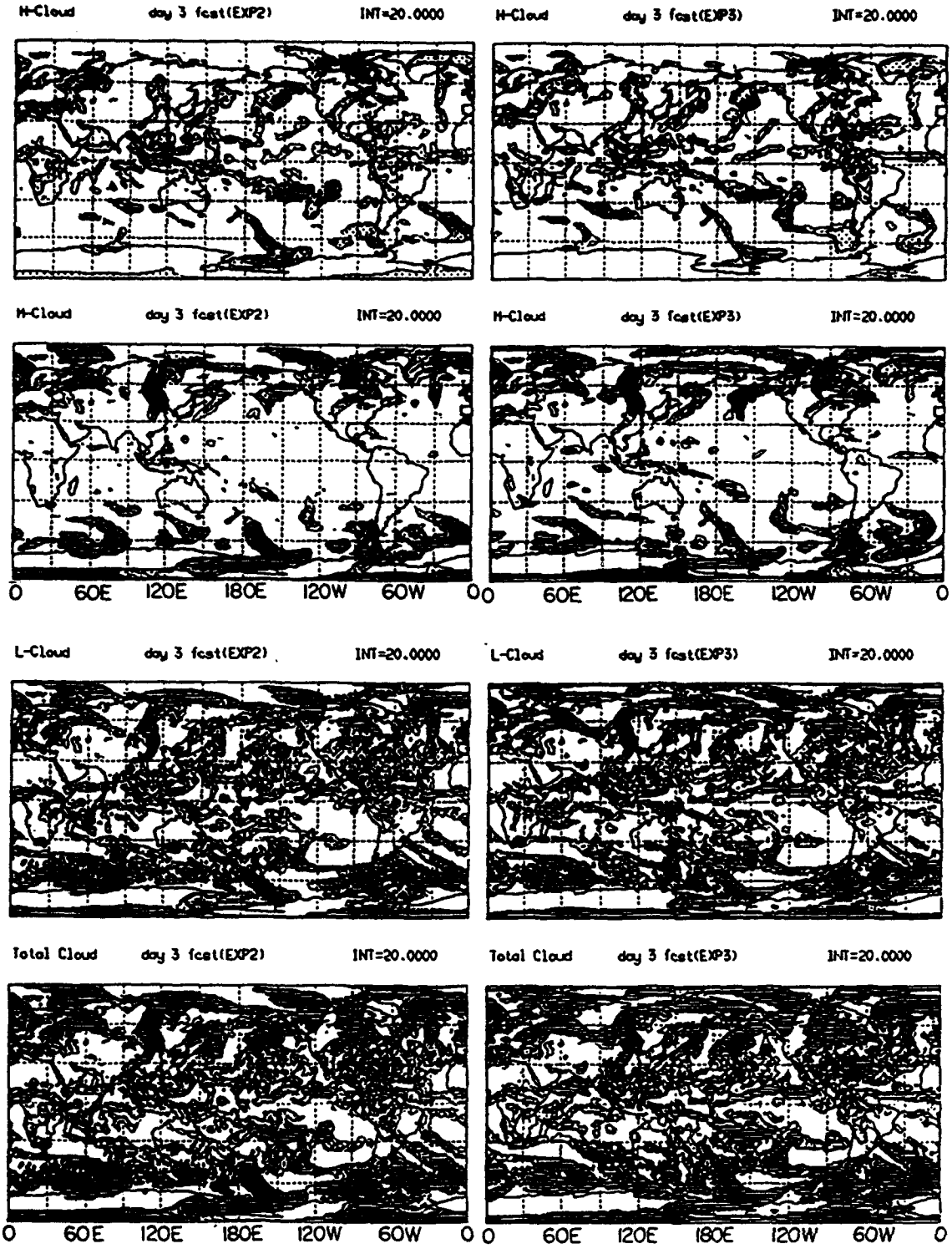

Figure 4.6(c) As Figure 4.6 (a) but for day 3 forecast.

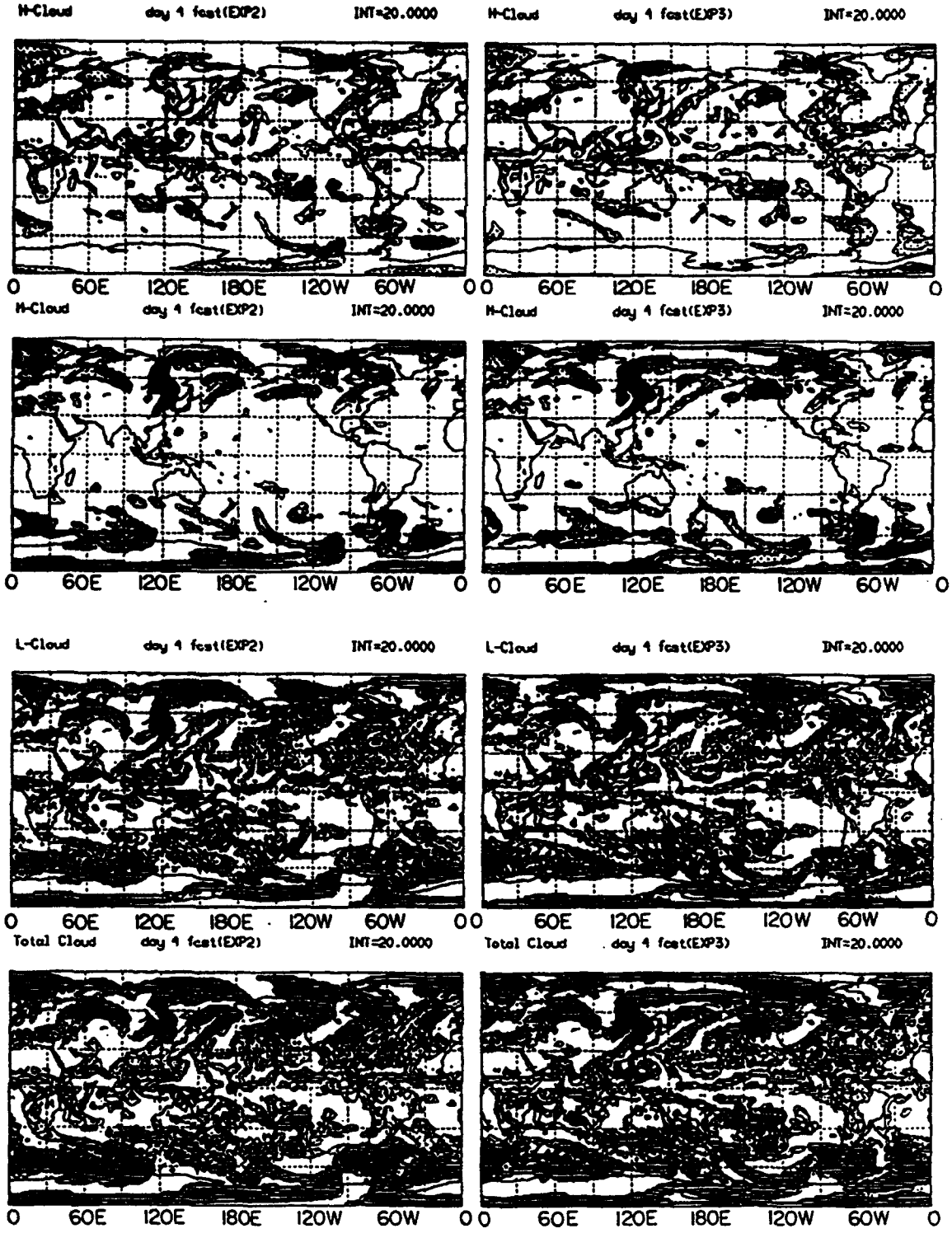

Figure 4.6(d) As Figure 4.6 (a) but for day 4 forecast.

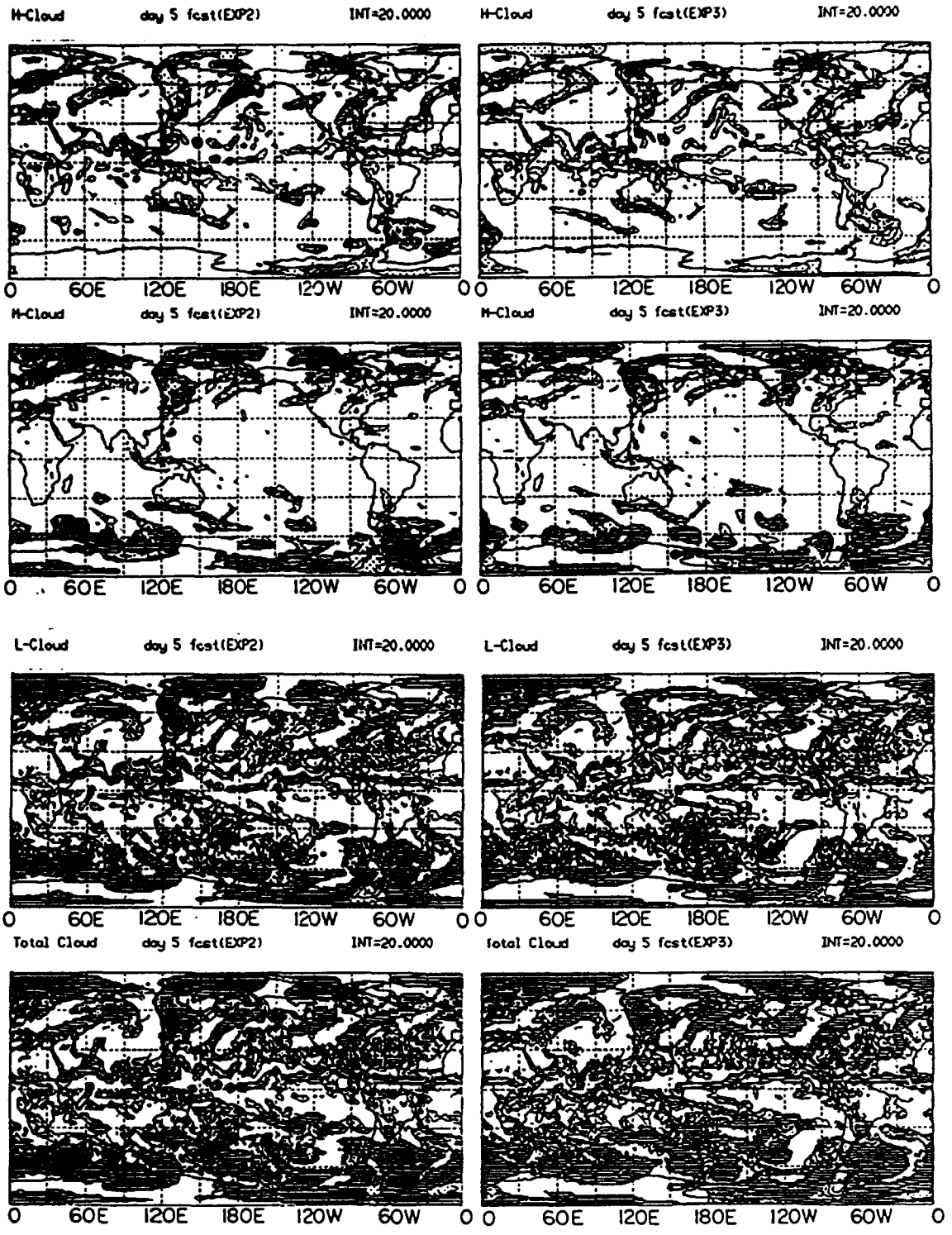

Figure 4.6(e) As Figure 4,6 (a) but for day 5 forecast.

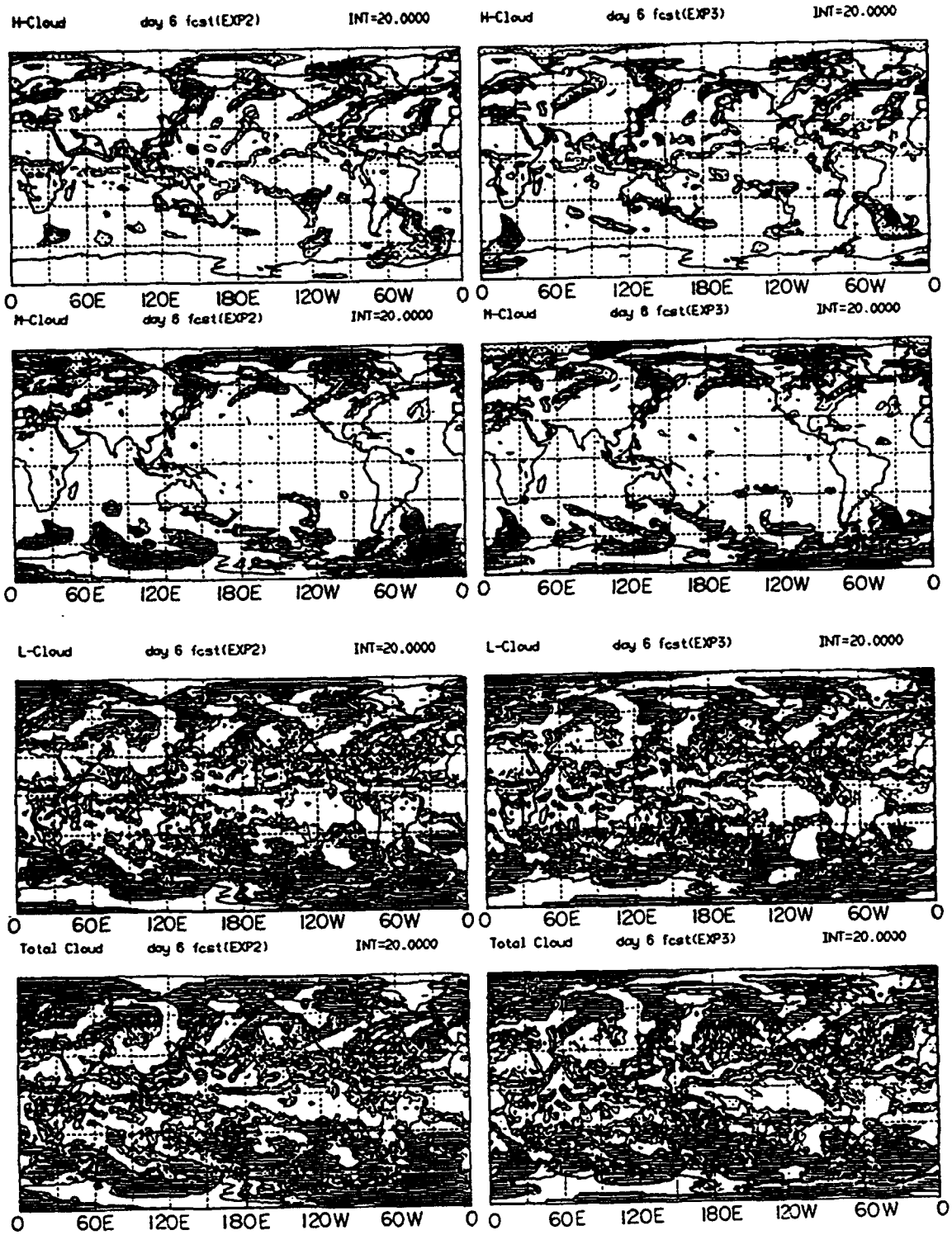

Figure 4.6(f) As Figure 4.6 (a) but for day 6 forecast.

Beyond day 3 no difference can be discerned in the cloud evolution between the two experiments. In other words, the impact of physical initialization on the explicit cloud scheme is negligible after 2 days.

4.2.4 Cloud predictive skills

In order to gauge the cloud forecast skill of the model, the root mean square error (RMSE) is computed. We define RMSE as

$$\text{RMSE} = \left[\overline{(C^f - C^a)^2}\right]^{1/2}$$

where C^f and C^a denote the predicted and analyzed cloud cover, respectively, and the overbar represents a global average. In the calculation of persistence RMSE (PRMSE), C^f is replaced by the initial clouds.

Figure 4.7 plots the ratio of RMSE to PRMSE of the total cloud cover as a function of forecast time for the control run, EXP1, EXP2 and EXP3. This figure clearly shows that EXP1 has some predictive skill up to day 4. The control run maintains the same level of skill only out to day 2.5. Beyond these limits the RMSE ratio exceeds 1 indicating that the persistence forecast is better. The other experiments consistently have a RMSE ratio greater than 1. This suggests that the physically initialized initial state with the implicit cloud scheme has the best predictive skill for cloud cover. All explicit experiments (EXP2, EXP3) drift to the climatological state within day 1 forecast. The graph shows that the explicit cloud scheme has no predictive skill for both initial conditions. This supports our earlier finding that the explicit scheme has a very irregular behavior and needs further investigation.

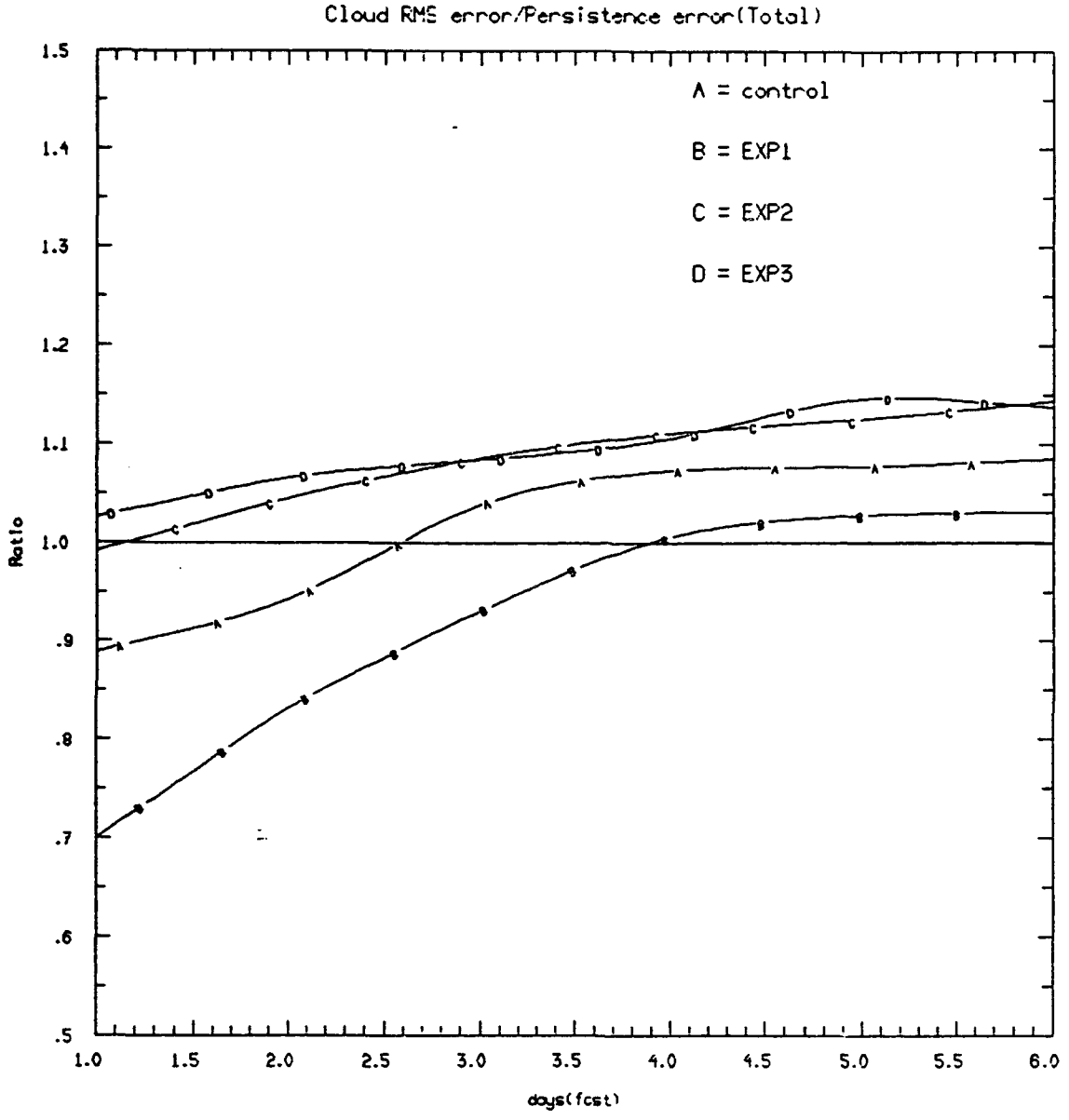

Figure 4.7 The ratio of RMSE to PMRSE of the total cloud cover as function of forecast time for the control run (A), EXP1(B), EXP2(C) and EXP3 (D).

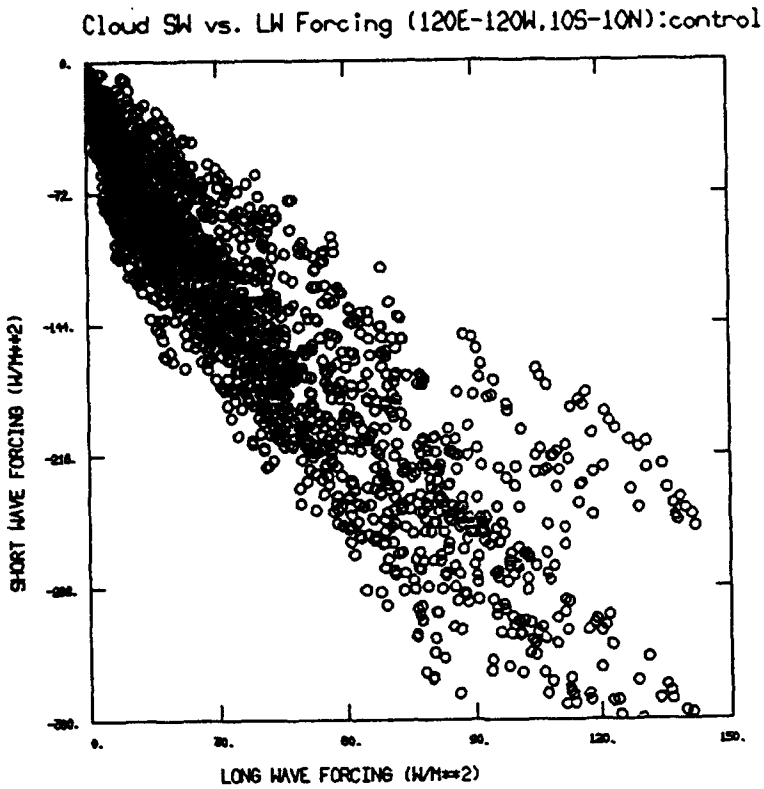

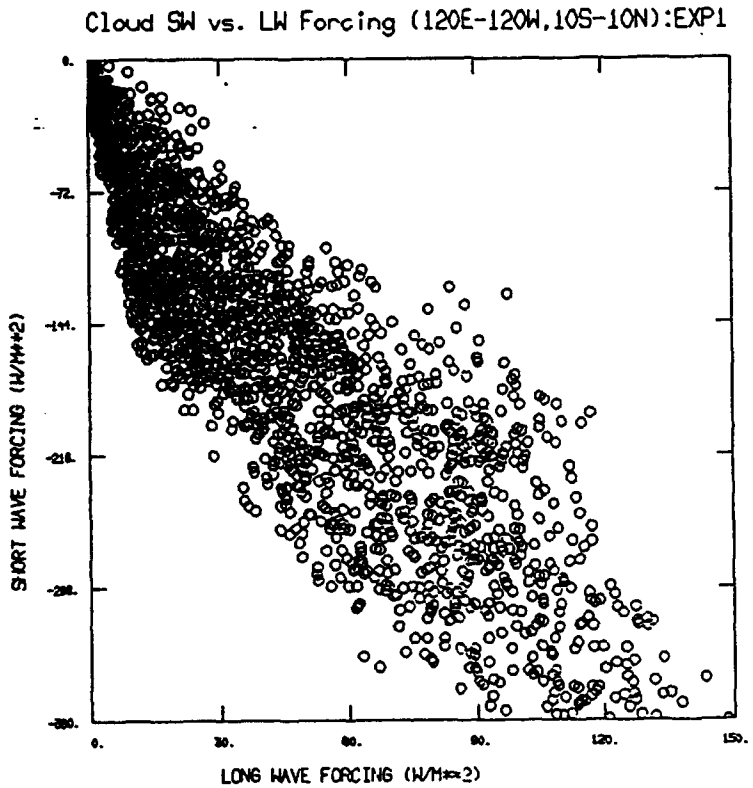

Figure 4.8 Scatter diagram of cloud shortwave forcing versus longwave forcing averaged for 6 day forecast over the tropical Pacific (120E-120W, 10S-10N) with the control run (top) and EXP1(bottom).

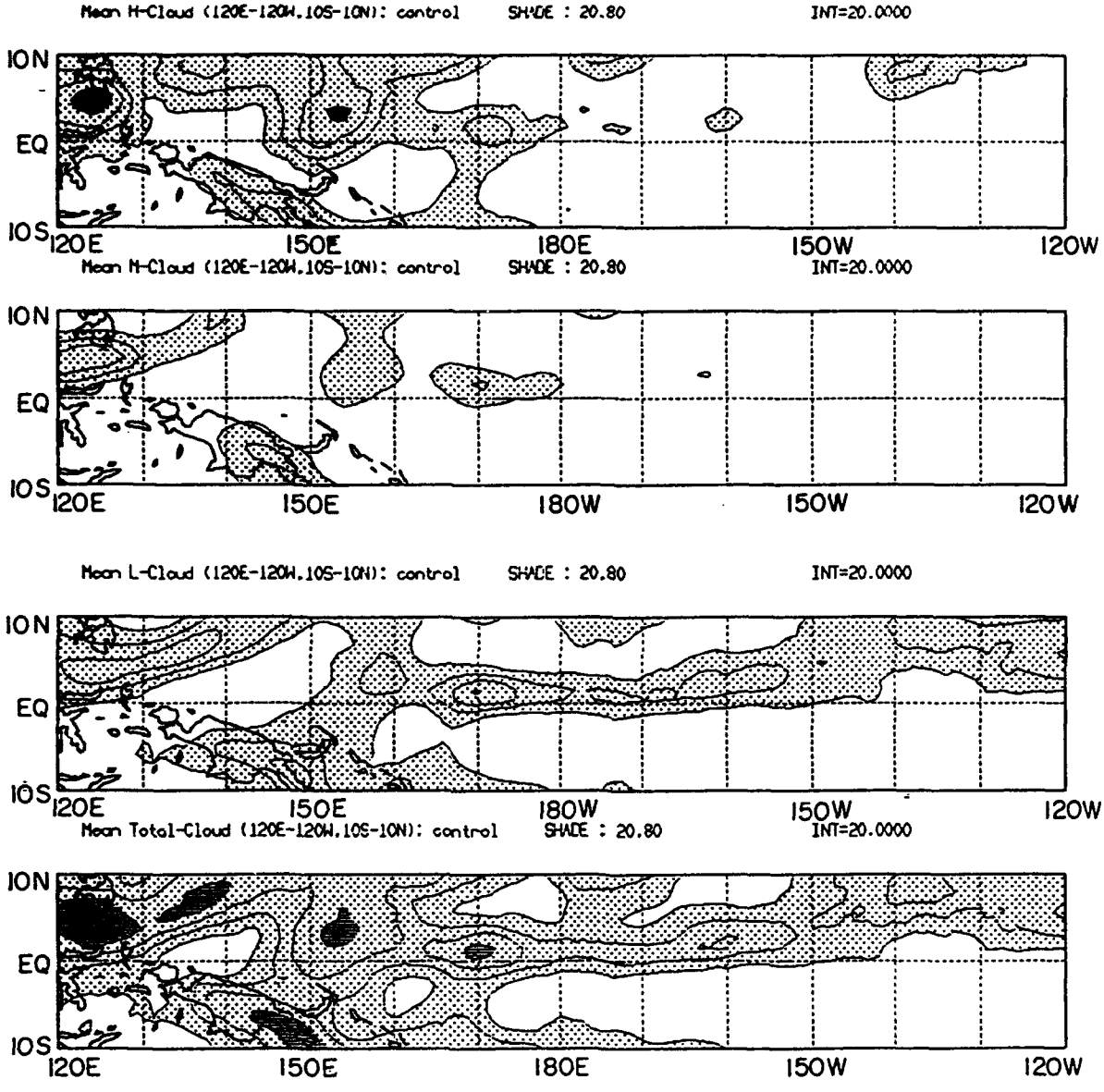

Figure 4.9(a) Distribution of the mean high, middle, low and total clouds for 6 days forecast over the tropical Pacific (120E-120W, 10S-10N) with the control run. Contour interval is 20%. Values between 20% and 80% are shaded; values above 80% are shaded.

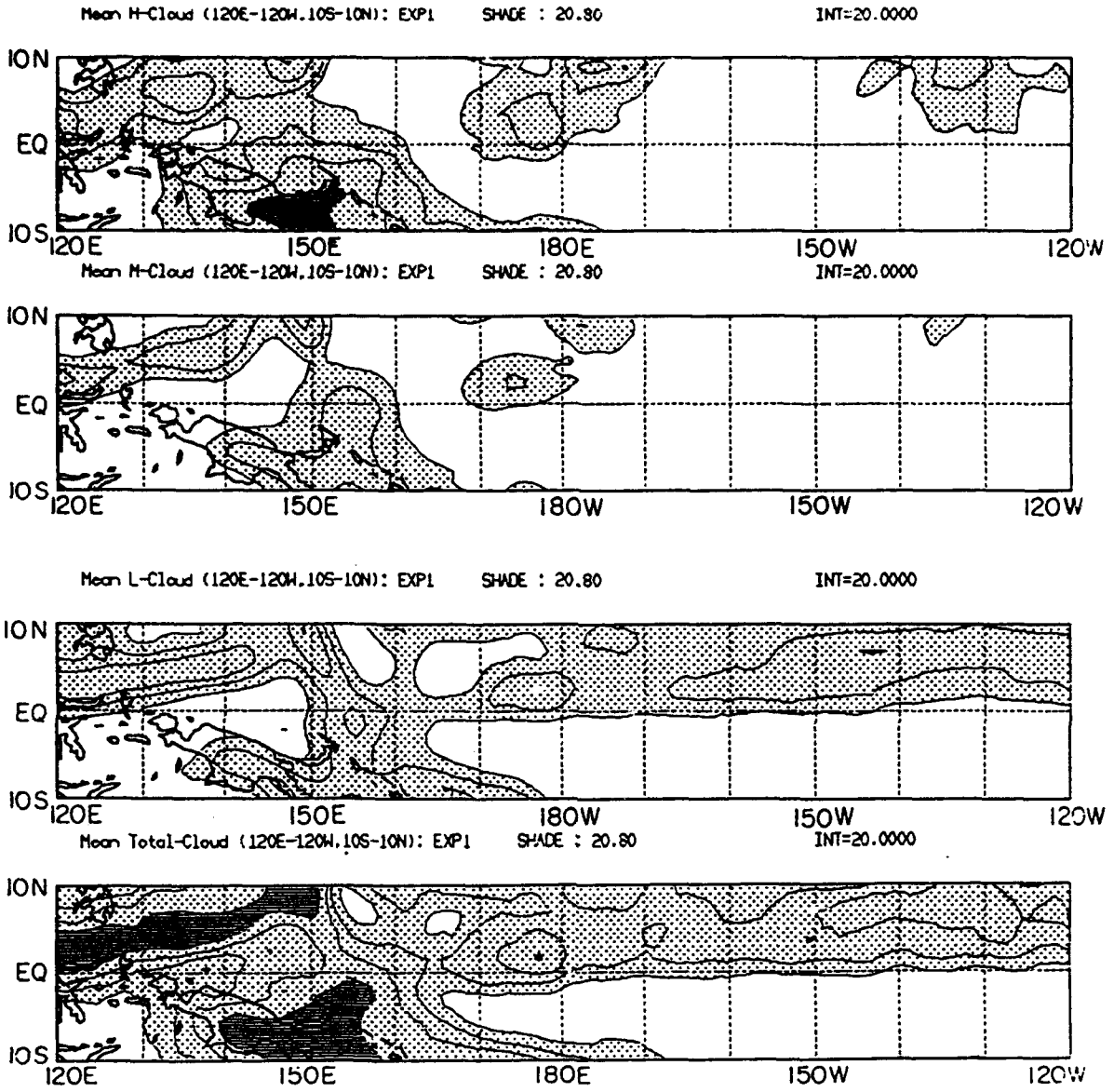

Figure 4.9(b) As Figure 4.9 (a) but for the EXP1.

linear fit is 0.92 for the control run and 0.91 for EXP1. These underestimate the 0.96 correlation computed from ERBE observations. The cloud forcing slopes are found to be -2.5 for both experiments. This slope is steeper than that in ERBE observations (-1.2). We attribute this difference to the fact that our values are from a single 6 day forecast rather than from monthly mean observations. This discrepancy also leads to a large difference with the magnitude of cloud forcings between the experiments and observations i.e., 360 W/m^2 (shortwave), 150 W/m^2 (longwave) for both experiments; 150 W/m^2 (shortwave), 120 W/m^2 (longwave) for observations. There are a few subtle differences that can be discerned from Figure 4.8 between the control and EXP1. In Figure 4.8 (top) note the small conglomeration of points over relatively small negative shortwave forcing ranging -144 to -288 W/m^2 and relatively large longwave forcing ranging 90 to 120 W/m^2. This suggests a significant amount of low clouds in the control experiment forecast. This is substantiated by Figure 4.9(a). Similarly, in Figure 4.8 (bottom) notice that there is a similar kind of conglomeration of points as before but over relatively small negative shortwave forcing ranging 0 to 144 W/m^2 and relatively small longwave forcing ranging 0 to 30 W/m^2. This indicates that EXP1 has more high clouds in its forecast. Figure 4.9(b) supports this contention.

CHAPTER V

CONCLUSIONS

In this study extensive work on cloud forecasts has been carried out. Two distinct cloud parameterizations have been examined in terms of both representativeness and predictive skill. One of these is the classical implicit method and the other an explicit method which carries certain cloud variables as prognostic variables. For each method two forecasts were made: one from physically initialized data and the other from initial conditions not subjected to physical initialization. These experiments provide the basis for an evaluation of the implicit and explicit schemes. From these experiments we also assess the impact of the initial data on the cloud forecast. Based upon results from the four experiments the following conclusions can be drawn:

1) The initial cloudiness of the physically initialized data set was in close agreement with the observed cloudiness. In the tropics it shows a remarkable improvement in the cloud cover. Cloud amounts of the physically initialized data are consistently higher than those of the normal data set in both hemispheres. The distribution of initial cloudiness shows that the physically initialized data is more representative in terms of a) the total cloud amount, b) the deep convective cloud associated with ITCZ and SPCZ, over active convective areas such as the western

Pacific, northeast of Australia, and over northern part of South America, and c) the high and low cloud amount in the middle latitudes.

2) The physically initialized data set has shown a major reduction in the spin-up time of high, middle and low clouds with the implicit cloud scheme.

3) The response of the explicit scheme to physically initialized data was very irregular. There was an initial decay of the high and middle clouds and an initial growth of low clouds before stabilization. Overall, high and middle clouds in both explicit experiments tend to decrease over the tropics during the forecast. Beyond day 3 no difference is noticed in the cloud evolution between the experiments with and without the physical initialization. Detailed study of the explicit cloud scheme is an avenue for further research.

4) The physically initialized initial state with the implicit cloud scheme has the best predictive skill (up to day 4). The normal initial state with the implicit cloud scheme maintains the same level of skill only up to day 2.5. All explicit experiments drift to the climatological state within day 1 of the forecast.

5) There is a strong negative correlation between the cloud shortwave forcing and longwave forcing (i.e., - 0.92 for the normal initial data and - 0.91 for the physically initialized data). This is in good agreement with the ERBE observations of - 0.96. Furthermore it is found that the implicit scheme without the physical initialization tends to produce a larger population of low clouds (small negative shortwave forcing, large longwave forcing), while that with the

physical initialization produces a larger population of high clouds (small negative shortwave forcing, small longwave forcing).

References

Bengtsson, L., M. Kanamitsu, P. Källberg and S. Uppala, 1982: FGGE 4-dimensional data assimilation at ECMWF. *Bull. Amer. Met. Soc.*, 63, 29-43.

Betts, A.K., 1973: Non-precipitating cumulus convection and its parameterization. *Quart. J. Roy. Met. Soc.*, 99, 178-196.

Businger, J.A., J.C. Wyngard, Y, Izumi and E.F. Bradley, 1971: Flux profile relationship in the atmospheric surface layer. *J. Atmos. Sci.*, 28, 181-189.

Chang, C.B., 1979: On the influence of solar radiation on diurnal variation of surface temperatures on African disturbances. Rep. No. 79-3, Dept. of Meteor., The Florida State University, 157 pp.

Chang, L.W., 1978: Determination of surface flux of sensible heat, latent heat, and momentum utilizing the Bulk Richardson number. *Pap. Meteorol. Res.* 1, 16-24.

Chou, M.D., 1984: Broadband water vapor transmission functions for atmospheric IR flux computations. *J. Atmos. Sci.*, 41, 1775-1778.

Chou, M.D. and Peng, L., 1983: A parameterization of the absorption in the 15 μm CO_2 spectral region with application to climate sensitivity studies. *J. Atmos. Sci.*, 40, 2183-2192.

Davies, R., 1982: "Documentation of the Solar Radiation Parameterization in the GLAS Climate Model". NASA Tech. Memo. 83961. Goddard Space Flight Cent., Greenbelt, Maryland.

Harshvardhan, Davies, R., Randall, D.A., and Corsetti, T.G., 1987: A fast radiation parameterization for atmospheric circulation models. *J. Geophys. Res.*, 92, 1009-1016.

Harshvardhan, and Corsetti, T.G., 1984: "Longwave Parameterization for the UCLA/GLAS GCM", NASA Tech. Memo. 86072. Goddard Space Flight Cent., Greenbelt, Maryland.

Heymsfield, A.J., 1977: Precipitation development in stratiform ice clouds: A microphysical and dynamical study. *J. Atmos. Sci.*, 34, 367-381.

Hoke, J.E. and Anthes, R.A., 1976: The initialization of numerical models by dynamic initialization technique', *Mon. Wea. Rev.*, 104, 1551-1556.

Joseph, J.H., Wiscombe, W.J. and Weinman, J.A., 1976: The delta-Eddington approximation of radiative flux transfer, *J. Atmos. Sci.*, 33, 2452-2459.

Kanamitsu, M., K. Tada, K. Kudo, N. Sato and S. Isa, 1983: Description of the JMA operational spectral model. *J. Met. Soc. Japan*, 61, 812-828.

Kanamitsu, M., 1975: On numerical prediction over a global tropical belt. Report No. 75-1, Dept. of Meteorology, Florida State University, Tallahassee, Florida 32306, pp. 1-282.

Krishnamurti, T.N., G. Rohaly and H.S. Bedi 1994: On the improvement of precipitation forecast skill from Physical Initialization. to appear in *Tellus*.

Krishnamurti, T.N., H.S. Bedi and K. Ingles, 1993: Physical initialization using SSM/I rain rates. *Tellus*, 45A, 247-269.

Krishnamurti, T.N., J. Xue, H.S. Bedi, K. Ingles and D. Oosterhof, 1991: Physical initialization for numerical weather prediction over the tropics. *Tellus*, 43AB, 53-81.

Krishnamurti, T.N., A. Kumar, K.S. Yap, A.P. Dastoor, N. Davidson and J. Sheng, 1990: Performance of a high-resolution mesoscale tropical prediction model. *Advances in Geophysics*, Vol. 32, Academic Press, pp. 133-286.

Krishnamurti, T.N., H.S. Bedi, W. Heckley and K. Ingles, 1988: Reduction of the spinup time for evaporation and precipitation in a spectral model. *Mon. Wea. Rev.*, 116, 907-920.

Krishnamurti, T.N., H.S. Bedi, K. Ingles, A. Weiner, K. Kuma, K.A. Campana and M. Kimoto, 1988: Comparison of cloud cover from global models and ISCCP data sets. Report prepared for the forth session of the CAS/JSC-WGNE, Toront, 16-30, September, 1988.

Krishnamurti, T.N., K. Ingles, S. Cocke, R. Pasch and T. Kitade, 1984: Details of low latitude medium range numerical weather prediction using a global spectral model II. Effect of orography and physical initialization. *J. Meteor. Soc. Japan*, 62, 613-649.

Krishnamurti, T.N., S. Low-Nam and R. Pasch, 1983: Cumulus parameterization and rainfall rates II. *Mon. Wea. Rev.*, 111, 816-828.

Kuo, H.L., 1965: On formation and intensification of tropical cyclones through latent heat release by cumulus convection. *J. Atmos. Sci.*, 22, 40-63.

Kuo, H.L., 1974: Further studies of the parameterization of the influence of cumulus convection on large scale flow. *J. Atmos. Sci.*, 31, 1232-1240.

Lacis, A.A., and Hansen, J.E., 1974: A parameterization for the absorption of solar radiation in the Earth's atmosphere, *J. Atmos. Sci.*, 31, 118-133.

Le Treut, H., 1990: Sensitivity and validation studies with a prognostic cloud generation scheme. ECMWF/WCRP Workshop. Clouds, Radiative Transfer and the Hydrological Cycle, 12-15, November, 1990, 223-239.

Le Treut, H. and Z.X. Li, 1988: Using Meteostat data to validate a prognostic cloud water scheme. *Atmos. Res.*, 21, 273-292.

Louis, J.F., 1979: A parametric model of vertical eddy fluxes in the atmosphere. *Bound. Layer. Meteor.*, 17, 187-202.

Mannoji, N., 1993: An explicit cloud predicting scheme in the Florida State University Global Spectral Model. Submitted for publication to *J. Meteor. Soc. Japan.*

Mathur, M.B., H.S. Bedi, T.N. Krishnamurti, M. Kanamitsu and J.S. Wollen, 1992: Use of satellite-derived rainfall for improving tropical forecasts, *Mon. Wea. Rev.*, 120, 2540-2560.

Ogura, Y. and H. Cho, 1973: Diagnostic determination of cumulus cloud populations from observed large-scale variables. *J. Atmos. Sci.*, 30, 1276-1286.

Platt, C.M.R. and Harshvardhan, 1988: Temperature dependence of cirrus extinction: implications for climate feedback. *J. Geogr. Res.*, 93, 11051-11058.

Pudykiewicz, J., R. Benoit and J. Mailhot, 1992: Inclusion and verification of a predictive cloud-water scheme in a regional numerical weather prediction model. *Mon. Wea. Rev.*, 120, 612-626.

Ramanathan, V., and W. Collins, 1991: Thermodynamic regulation of ocean warming by cirrus clouds deduced from observations of the 1987 El Niño. *Nature*, 351, 27-32.

Rodgers, C.D., 1968: Some extensions and applications of the new random model for molecular band transmission, *Q. J. R. Meteor. Soc.*, 94, 99-102.

Sagan, C. and J.B. Pollack, 1967: Anisotropic nonconservative scattering and the clouds of Venus. *J. Geogr. Res.*, 172, 469-477.

Slingo, J.M., 1987: The development and verification of a cloud prediction scheme for the ECMWF model. *Q. J. Roy. Met. Soc.*, 113, 899-927.

Smith, R.N.B., 1990: A scheme for predicting layer clouds and their water content in a general circulation model. *Quart. J. Roy. Met. Soc.*, 116, 435-460.

Starr, D.O.C. and S.K.Cox, 1985: Cirrus clouds. Part I: A cirrus cloud model. *J. Atmos. Sci.*, 42, 2663-2681.

Stephens, G.L., 1984: The parameterization of radiation for numerical weather prediction and climate models. *Mon. Wea. Rev.*, 112, 826-867.

Stephens, G.L., 1978: Radiation profiles in extended water clouds. II: Parameterization schemes. *J. Atmos. Sci.*, 35, 2123-2132.

Approved for public release;
distribution unlimited.

Sundqvist, H., E. Berge and J.E. Kristj'nsson, 1989: Condensation and cloud parameterization studies with a mesoscale numerical weather prediction model. *Mon. Wea. Rev.*, 117, 1641-1657.

Sundqvist, H., 1978: A parameterization scheme for non-convective condensation including prediction of cloud water content. *Quart. J. Roy. Met. Soc.*, 104, 677-690.

Tiedtke, M., 1993: Representation of clouds in large-scale models. *Mon. Wea. Rev.*, 121, 3040-3061.

Tiedtke, M., 1991: Aspect of cumulus parameterizaion. ECMWF seminar on tropical extra-tropical interactions, Reading, U.K., 10-14 Sept.1990, 441-466.

Tiedtke, M., 1984: The sensitivity of the time-mean large-scale flow to cumulus convection in the ECMWF model. Workshop on convection in large-scale numerical models. ECMWF, 28 Nov. - 1 Dec. 1983, 297-316.

Wallace, J.M., S. Tibaldi and A.J. Simmons, 1983: Reduction of systematic forecast errors in the ECMWF model through the introduction of envelope orography. *Quart. J. Roy. Met. Soc.*, 109, 683-718.

Warren, S.G., C.J. Hahn, J. London, R.M. Chervin and R.L. Jenne, 1986: Global distribution of total cloud cover and cloud type amounts over land. NCAR Technical Note TN-273+STR, National Center for Atmospheric Research, Boulder, CO, 29 p. - 200 plates.

Yanai, M., S. Esbensen and J.H. Chu, 1973: Determination of bulk properties of tropical cloud clusters from large-scale heat and moisture budgets. *J. Atmos. Sci.*, 30, 611-627.

AIR FORCE OF SCIENTIFIC RESEARCH (AFSC)
NOTICE OF TRANSMITTAL TO DTIC
This technical report has been reviewed and is approved for public release IAW AFR 190-12
Distribution in unlimited.
Joan Boggs
STINFO Program Manager